NASA Contractor Report 168059

THE STRUCTURE OF PARTICLE-LADEN JETS AND NONEVAPORATING SPRAYS

J-S. Shuen, A. S. P. Solomon, Q-F. Zhang and G. M. Faeth

The Pennsylvania State University
University Park, Pennsylvania

February 1983

Prepared for

NATIONAL AERONAUTICS AND SPACE ADMINISTRATION
Lewis Research Center
Under Grant NAG3-190

The Structure of Particle-Laden Jets and Nonevaporating Sprays

SUMMARY

The first phase of a study of the structure of sprays, limited to the properties of particle-laden jets and nonevaporating sprays, is described. Several models of these processes were developed. Model performance was evaluated by comparison of predictions with existing measurements in particle-laden jets, as well as with new measurements in nonevaporating sprays completed during this investigation. Analysis and measurements were limited to the dilute portions of the flows, where the volume fraction of the continuous phase was greater than 99.1%.

Three models of the process were developed: (1) a locally homogeneous flow (LHF) model, where slip between the phases was neglected; (2) a deterministic separated flow (DSF) model, where slip was considered but effects of particle/drop dispersion by the turbulence were ignored; and (3) a stochastic separated flow (SSF) model, where effects of interphase slip and turbulent dispersion were considered using random sampling for turbulence properties in conjunction with random-walk computations for particle motion. All three models used a k-ε model which was extensively evaluated for constant and variable density single-phase jets during earlier work in this laboratory.

The new spray experiments employed vacuum pump oil--to insure negligible evaporation. The sprays were produced by an air-atomizing injector. Mean and fluctuating velocities and Reynolds stress were measured in the continuous phase using laser Doppler anemometry. Liquid mass fluxes were measured by isokinetic sampling. Drop sizes were measured by slide impaction.

The LHF and DSF models did not provide very satisfactory predictions over the present data base. The DSF model generally underestimated the rate of spread of the dispersed phase as a result of ignoring effects of turbulent dispersion. The LHF model provided reasonably good predictions for flows containing tracer-like particles, but was unsatisfactory for most practical flows. In earlier evaluations, LHF models generally overestimate the rate of spread of dispersed phases due to neglect of slip. Similar behavior was observed during this study for particle-laden jets, however, the LHF model underestimated spread rates for the present nonevaporating sprays. This indicates that LHF models do not always provide an upper bound on the rate of development of dilute particle-laden flows as suggested in the past.

In contrast to the other models, the SSF model provided reasonably good predictions over the data base. While this result is encouraging, uncertainties in initial conditions for much of the data limits the thoroughness of the evaluation of the SSF model. Some effects of particles on turbulence properties were observed at high particle mass loadings. Treatment of such dense particulate flow effects will require extension of the present SSF model. The SSF approach, however, appears

to provide an attractive formulation for treating nonlinear interphase transport processes in particle-laden turbulent flows. Current work in this laboratory is considering extension of the method to evaporating sprays.

TABLE OF CONTENTS

NOMENCLATURE

Symbol	Description
a	acceleration of gravity
C	particle concentration
C_D	drag coefficient
C_i	parameters in turbulence model
d	injector diameter
d_p	particle diameter
f	mixture fraction
G_p	particle mass flux
k	turbulence kinetic energy
L_e	dissipation length scale
m_p	particle mass
$\dot{m}_o$	injector flow rate
$\dot{M}_o$	injector thrust
$\dot{n}_i$	number of particles per unit time in group i
n	number of particle groups
Re	Reynolds number
r	radial distance
S_ϕ	source term
$S_{p\phi}$	particle source term
t	time
t_e	eddy lifetime
t_t	particle transit time
u	axial velocity
$\vec{u}_p$	particle velocity vector
v	radial velocity

Symbol	Description
v^o	Favre radial velocity
w	tangential velocity
x	axial distance
$\vec{x}_p$	particle position vector
$\Delta\vec{x}_p$	path length of particles in an eddy
Δt	time of particle residence in an eddy
ε	rate of dissipation of turbulence kinetic energy
μ_t	turbulent viscosity
ρ	density
τ	particle relaxation time
σ_i	turbulent Prandtl/Schmidt number
ϕ	generic property

Subscripts

c	centerline quantity
p	particle property
o	injector exit condition
∞	ambient condition

Superscripts

$( )'$	fluctuating quantity
$(\bar{})$	time mean value
$(\vec{})$	vector quantity
$( )''$	instantaneous quantity

1. INTRODUCTION

The objective of this investigation was to complete measurements of spray structure, useful for evaluation of models of the process. The tests considered nonevaporating sprays, generated by an air-atomizing injector, in a still environment. This arrangement has simple geometry and well-defined boundary conditions, which facilitates model evaluation. Furthermore, nonevaporating sprays highlight effects of drops on the properties of the continuous phase and effects of drop dispersion by turbulence in sprays, while minimizing complications due to density variations in the flow. The new data was also used to begin model evaluation considering methods typical of recent spray models.

Existing data on the mean and turbulent structure of nonevaporating sprays is limited. A recent review discusses early work in the field [1].* Subsequently, Alpert and Mathews [2,3] report predictions and measurements for nonevaporating sprays having configurations encountered in sprinkler systems. Due to the complexity of this geometry and the limited measurements available, however, they suggest that additional measurements and analysis would be desirable. Yule et al. [4] report measurements in nonevaporating sprays from a twin-fluid injector in a coflowing stream. Measurements of particle size were undertaken using a laser tomographic light-scattering technique while mean drop and continuous-phase velocities were measured using laser Doppler anemometry (LDA). These measurements are currently being employed to evaluate spray models in this laboratory. The results of this comparison will be reported in the future.

The present investigation supplements the measurements of Yule et al. [4] considering the simpler limiting case of a spray in a stagnant environment. Mean and fluctuating velocities of the continuous phase were measured, using LDA techniques. Drop sizes were measured using the Fraunhofer diffraction and the slide impaction methods. Liquid fluxes in the spray were found with an isokinetic sampling probe.

These new measurements, as well as existing measurements of the structure of particle-laden jets, were employed to initiate evaluation of models to predict spray structure. Since these flows only involve interphase momentum exchange, modeling efforts concentrated on effects of turbulent fluctuations on momentum exchange between the phases as well as the dispersion of the dispersed phase by turbulent fluctuations.

The structure of sprays and other particle-laden flows is generally influenced by turbulent dispersion of the discrete phase. Turbulent dispersion of particles is examined during this investigation

---

*Numbers in brackets denote references.

by comparing predictions of several theoretical models with existing measurements. The study emphasized solid-particle-laden jets in a still environment. These results are also of interest for spray modeling, however, since the geometry approximates near injector conditions while consideration of solid particles avoids complications due to polydisperse drop size distributions and drop coalescence.

Past models of turbulent particle-laden jets often consider two limiting cases instead of treating turbulent particle dispersion [1]. At one limit the particles and the continuous phase are assumed to have equal rates of turbulent diffusion. The locally homogeneous flow (LHF) approximation provides a consistent formulation of this limit. This implies that interphase transport rates are infinitely fast, so that both phases have the same velocity at each point in the flow. The LHF approximation provides best results for flows containing small particles, where characteristic response times of particles are small in comparison to characteristic times of turbulent fluctuations. LHF models have been extensively evaluated during earlier work in this laboratory, but only yielded accurate predictions for particle sizes smaller than most practical applications [5-7].

Turbulent particle dispersion is neglected entirely at the other limit. This implies that particles follow deterministic trajectories since they only interact with mean properties of the continuous phase, yielding a deterministic separated flow (DSF) model. Such an approximation is appropriate for flows containing large particles, where characteristic particle response times to flow disturbances are large in comparison to characteristic turbulent fluctuation times. Several spray models have been proposed along these lines, e.g., El Banhawy and Whitelaw [8], Mongia and Smith [9], and Boyson and Swithenbank [10], among others [1]. Due to the complexities of sprays and uncertainties in initial conditions, however, the value of DSF models has not been clearly established as yet.

Most practical particle-laden flows exhibit properties between these limits and require consideration of turbulent particle dispersion. Early dispersion models, discussed by Yuu et al. [11] apply a gradient diffusion approximation with empirical correlations of turbulent particle exchange coefficients. This approach is not practical, however, since such exchange coefficients are influenced by both particle and turbulence properties--requiring excessive effort to accumulate a data base sufficient for general application of the method.

Several recent studies of turbulent particle dispersion use stochastic separated flow (SSF) methods to circumvent the limitations of the gradient diffusion approach. Stochastic analysis requires an estimate of the mean and turbulent properties of the

continuous phase. Particle trajectories are then computed by random sampling to find instantaneous continuous phase properties. Mean and fluctuating particle properties are found by Monte Carlo methods--where a statistically significant number of particle trajectories are averaged to obtain system properties.

SSF models have been applied to particle-laden jets. Yuu et al. [11] use empirical correlations of mean and turbulent properties for SSF analysis of their particle dispersion measurements. Gosman and Ioannides [12] propose a more comprehensive approach, where flow properties for the stochastic calculations are computed with a k-ε turbulence model. This approach is examined here, after only minor modification.

In the following, the models are described first of all, followed by initial evaluation using existing measurements for particle-laden jets. Experimental methods used for measurements in nonevaporating sprays are then discussed. The report concludes with an evaluation of the models using the spray measurements. Other reports of the findings of this investigation can be found in Refs. [13-15].

2. THEORY

2.1 General Description

A k-ε turbulence model was used to find the properties of the continuous phase for all models, since this approach has been thoroughly calibrated for both constant and variable density jets [5-7,16]. All conditions to be considered can be modeled as steady axisymmetric boundary layer flows. Nozzle exit Mach numbers were less than 0.3; therefore, kinetic energy and viscous dissipation of the mean flow, as well as gas density variations, were neglected with little error. Other assumptions will be described when introduced since they differ for each model.

2.2 LHF Model

The formulation of the LHF model corresponds to the general treatment of the continuous phase for all three models. The LHF approximation implies that both phases have the same velocity at each point in the flow, i.e., local thermodynamic equilibrium is maintained. Therefore, the flow corresponds to a variable density single-phase fluid due to changes in particle concentration even though the density of each phase is constant. Following past work [5-7,16] the governing equations are written in Reynolds averaged form, as follows:

$$\frac{\partial}{\partial x}\left(\bar{\rho}\bar{u}\phi\right) + \frac{1}{r}\frac{\partial}{\partial r}\left(r\bar{\rho}\bar{v}^{o}\phi\right) = \frac{1}{r}\frac{\partial}{\partial r}\left(r\,\frac{\mu_t}{\sigma_\phi}\,\frac{\partial\phi}{\partial r}\right) + S_\phi \qquad (1)$$

where

$$\bar{\rho}\bar{v}^{o} = \bar{\rho}\bar{v} + \overline{\rho' v'} \tag{2}$$

The parameters ϕ and S_ϕ appearing in Eqs. (1) and (2) are summarized in Table 1, along with the appropriate empirical constants. The empirical constants were established for single-phase flows [5-7,16]. They were not changed during present calculations for particle-laden jets. The turbulent viscosity was calculated from the turbulent kinetic energy and its rate of dissipation as follows:

$$\mu_t = C_\mu \bar{\rho} k^2/\varepsilon \tag{3}$$

For present assumptions, the instantaneous particle concentration and flow density are only functions of mixture fraction--corresponding to the equilibrium state reached when f and (1-f) kg of injected and ambient fluid, respectively, are adiabatically mixed. This yields

$$C/C_o = f \quad ; \quad \rho^{-1} = f/\rho_o + (1-f)/\rho_\infty \tag{4}$$

Since C and ρ^{-1} are linear functions of f in the domain $0 \leq f \leq 1$, their mean values can be found by substituting $\bar{f}$ in Eq. (4). In this instance, it is not necessary to solve a transport equation for mixture fraction fluctuations and to adopt a probability density function (PDF) for f--which is usually necessary during LHF analysis of sprays [5-7].

Ambient values of $\bar{u}$, $\bar{f}$, k and ε are all zero for the flows treated here. Gradients of these quantities are also zero at the axis.

Initial conditions varied over the data base. For the round jets and the spray, initial conditions were approximated as either slug flow or fully developed pipe flow.

When slug flow is assumed at the injector exit, initial conditions were prescribed similar to past work [5-7]. All properties were assumed to be constant, except for a shear layer having a thickness equal to 1 percent of the injector radius at the passage wall. The constant property portion of the flow was specified as follows:

$$x = 0 \quad , \quad r < 0.99d/2;$$

$$\bar{u}_o = \dot{M}_o/\dot{m}_o \quad , \quad \bar{f}_o = 1 \quad , \quad k_o = (0.02\bar{u}_o)^2 \quad ,$$

$$\varepsilon_o = 2.84 \times 10^{-5}\, \bar{u}_o^{\,3}/d \tag{5}$$

Table 1 Source Terms in Eq. (1)

ϕ	S_ϕ
1	0
$\bar{u}$	$\pm a\,(\rho_\infty - \bar{\rho})$
k	$\mu_t \left(\frac{\partial \bar{u}}{\partial r}\right)^2 - \bar{\rho}\varepsilon$
$\bar{f}$	0
ε	$C_{\varepsilon_1} \mu_t \frac{\varepsilon}{k} \left(\frac{\partial \bar{u}}{\partial r}\right)^2 - C_{\varepsilon_2} \bar{\rho} \frac{\varepsilon^2}{k}$

Notes:

1. Positive sign is used in $S_{\bar{u}}$ for vertical upward flow.

2. Turbulence model constants are assigned the following values:

   $C_\mu = 0.09$, $C_{\varepsilon_1} = 1.44$, $\sigma_k = 1.0$,

   $\sigma_\varepsilon = 1.3$, $\sigma_f = 0.7$, and

   $C_{\varepsilon_2} = 1.84$ (variable density flows) = 1.89 (constant density flows).

Equation (5) provides the inner boundary conditions of the shear layer until it reaches the jet axis. The initial variation of $\bar{u}$ and $\bar{f}$ is taken to be linear in the shear layer. Initial values of k and ϵ in the shear layer were found by solving their transport equations while neglecting convection and diffusion terms.

When fully-developed pipe flow was assumed at the injector exit, $\bar{f}_o$ was taken to be unity while $\bar{u}_o$ was obtained from the power law expressions provided by Schlicting [17]--allowing for variation of the power with Reynolds number. Initial values of k_o and ϵ_o were obtained from Hinze [18] for fully-developed pipe flow in the present Reynolds number range.

The calculations were performed using a modified version of GENMIX [19]. The computational grid was similar to past work [5-7]: 33 cross-stream grid nodes; streamwise step sizes limited to 6% of the current flow width or an entrainment increase of 10%--whichever was smaller.

2.3 DSF Model

Continuous Phase. Both separated flow models adopt the main features of the LHF model, but only for the gas phase. The particle/drop* phase is treated by solving Lagrangian equations of motion for the particles and then computing the source terms which appear in the governing equations for the gas phase due to interphase transport processes. This procedure corresponds to the particle-tracking or particle-source-in-cell methods used in most recent models of sprays [1-3,8-10]. With this approach, particles leaving the jet exit are divided into n groups, defined by initial position, velocity, and direction.

The void fraction of the flows was always greater than 99.1%; therefore, the volume occupied by the discrete phase was ignored with little error. Under these conditions it is also reasonable to neglect the effect of particle motion on turbulence properties--although exchange of mean momentum between phases was considered as noted earlier. The gas-phase density is constant, simplifying Eq. (1), and a solution for $\bar{f}$ is no longer needed since particle concentrations are found from the discrete phase solution.

The interaction between the discrete and continuous phases yields an additional source term in Eq. (1) for $\bar{u}$. This term is found by computing the net change in momentum of each particle group i as it passes through a computational cell j (only one index is needed to define a cell since the calculation is parabolic and each cell is defined by its radial position). This yields the following source term expression

---

*In the following, particle will denote drops (assumed to be spherical) as well as solid particles.

$$S_{\vec{pu}_j} = \sum_{i=1}^{n} \dot{n}_i \, m_{pi} \left[(\vec{u}_{pi})_{in} - (\vec{u}_{pi})_{out} \right]_j \tag{6}$$

where $\dot{n}_i$ is the number of particles per unit time in each group, and "in" and "out" denote conditions entering and leaving a computational cell.

The continuous-phase equations were solved in the same manner as the LHF model.

Discrete Phase. The main assumptions of the particle trajectory calculations are as follows: due to the high void fractions of the measurements, dilute-particle flow was assumed with drag equivalent to a single particle in an unbounded environment and negligible particle collision or coalescence when drops are considered; drag was treated empirically, assuming quasisteady flow for spherical particles; since $\rho_p / \rho > 200$ for conditions treated here, effects of virtual mass Bassett forces, Magnus forces, etc., can be neglected with little error; effects of turbulent fluctuations were neglected, similar to most separated flow models; and ambient conditions of the particles were taken to be local mean flow properties. The last two assumptions are characteristic of the DSF formulation [1-3,8-10] and will be relaxed for the SSF model. The remaining assumptions are typical of separated flow models of dilute sprays and are disucssed more completely elsewhere [1].

After adopting these assumptions, the position and velocity of each particle group is found by integrating

$$\frac{dx_{pi}}{dt} = u_{pi} \quad , \quad i = 1,2,3 \tag{7}$$

$$\frac{du_{pi}}{dt} = \left(\frac{3 \rho C_D}{4 d_p \rho_p} \right) (\bar{u}_i - u_{pi}) |\vec{\bar{u}} - \vec{u}_p| + a_i \quad , \quad i=1,2,3 \tag{8}$$

Particle Reynolds numbers did not reach the supercritical flow regime; therefore, the standard drag coefficient for solid spheres was approximated as follows [1]:

$$C_D = \frac{24}{Re} \left(1 + \frac{Re^{2/3}}{6} \right) \quad , \quad Re < 1000$$

$$= 0.44 \quad , \quad Re > 1000 \tag{9}$$

The particle motion equations, Eqs. (7) and (8), were solved at the same time as the gas-phase equations, in a stepwise fashion. A second-order finite difference algorithm was employed for these computations. The computations employed no less than 100 (particle-laden jets) and 400 (sprays) groups.

2.4 SSF Model

The SSF model involves finding trajectories of a statistically significant sample of individual particles as they move away from the injector and encounter a random distribution of turbulent eddies--using Monte Carlo methods. The treatment of the continuous phase was identical to the DSF model.

Key elements in the SSF model are the method used to specify eddy properties and the time of interaction of a particle and a particular eddy. The approach used to find these properties follows Gosman and Ioannides [12], but differs in some details. Properties were assumed to be uniform within each eddy and to change randomly from one eddy to the next. Particle trajectory computations were the same as the DSF model, involving solution of Eqs. (7) and (8); however, mean gas properties in these equations were replaced by the instantaneous properties of each eddy.

The properties of each eddy were found at the start of particle/eddy interaction by making a random selection from the probability density function (PDF) of velocity. Velocity fluctuations were assumed to be isotropic with a Gaussian PDF having a standard deviation of $(2k/3)^{1/2}$ and mean components $\bar{u}$, $\bar{v}$, 0. The cumulative distribution function for each velocity component was constructed and sampled. This involved randomly selecting three numbers in the range 0-1 and computing the velocity components for these three values of the cumulative distribution function.

A particle was assumed to interact with an eddy for a time which is the minimum of either the eddy lifetime or the transit time required for the particle to cross the eddy. These times were estimated assuming that the characteristic size of an eddy is the dissipation length scale.

$$L_e = C_\mu^{3/4} k^{3/2}/\varepsilon \tag{10}$$

Gosman and Ioannides [12] compute the eddy lifetime as $t_e = L_e/|\vec{u}'|$, however, we obtained better agreement with measurements using

$$t_e = L_e/(2k/3)^{1/2} \tag{11}$$

A portion of the present calculations employed the method proposed by Gosman and Ioannides to find the transit time. In this case, the transit time of a particle is found from the linearized equation of particle motion in a uniform flow (LSSF model)

$$t_t = -\tau \ln (1 - L_e/(\tau|\vec{u}'' - \vec{u}_p''|)) \tag{12}$$

where $\vec{u}'' - \vec{u}_p''$ is the velocity difference at the start of the interaction and τ_p is the linearized particle relaxation time

$$\tau = 4\, \rho_p d_p/(3\, C_D|\vec{u}'' - \vec{u}_p''|) \tag{13}$$

When $L_e > \tau|\vec{u}'' - \vec{u}_p''|$, the linearized stopping distance of the particle is smaller than the characteristic length scale of the eddy and Eq. (13) has no solution. In this case, the eddy has captured the particle and the interaction time is the eddy lifetime.

The linearization of the particle motion equation is an undesirable feature of LSSF model, since nonlinear effects are considered elsewhere in the analysis. Therefore, a second method was also used where particles were assumed to interact with an eddy as long as the time of interaction, Δt, and the distance of interaction $|\Delta \vec{x}_p|$, satisfied the following criteria (NSSF model)

$$\Delta t \leq t_e \quad , \quad |\Delta \vec{x}_p| \leq L_e \tag{14}$$

Particle capture by an eddy corresponds to ending the interaction with the first criterion while a particle traverses an eddy when the interaction is ended with the second criterion.

The remaining computations are similar to the DSF model, except that more particle trajectories must be considered to obtain statistically significant particle properties (generally 1000-2500 trajectories were used). A by-product of the additional calculations, however, is that the SSF models yield both mean and fluctuating particle properties. This provides an additional test of model performance.

3. MODEL EVALUATION: PARTICLE-LADEN JETS

3.1 Data Base

The data base used to develop and evaluate the particle-laden jet models is summarized in Table 2. The findings of Hinze [18] and Snyder and Lumley [20] were used for initial evaluation of the SSF model--similar to Gosman and Ioannides [12]. The other measurements, for particle-laden jets, were used for model evaluation.

Table 2 Summary of Measurements Used for Evaluation in Solid Particle-Laden Flows[a]

Source: Configuration	Loading Ratio[b]	Reynolds Number	Particles			Assumed Initial Condition[c]
			Type	Diameter (μm)	Density (kg/m^3)	
Hinze [18]: one-dimensional flow, isotropic turbulence.	Single particles	--	Theoretical	0	0	Uniform flow, no slip
Snyder and Lumley [20]: duct flow, grid-generated turbulence.	Single particles	11,000 (grid) 176,000 (channel)	hollow glass corn pollen glass copper	46.5 87 87 46.5	260 1,000 2,500 8,900	Uniform flow, no slip
Yuu et al. [11]: round jet.	0.0008-0.004	11,000-56,000	fly ash	20	2,000	Slug flow, estimated slip
McComb and Salih [21,22]: round jet.	Small	5,000-15,000	titanium dioxide tungsten	2.3 5.7	4,260 19,300	Slug flow, no slip
Laats and Frishman [23,24]: round jet.	0.3-1.4	66,000-137,000	corundum	17-80	4,022	Fully developed pipe flow, no slip
Levy and Lockwood [25]: round jet.	1.14-3.50	20,000	sand	215-1,060	2,250	Fully developed pipe flow, estimated slip

[a]Continuous phase was air at normal temperature and pressure. Round jets were injected into still air.

[b]Ratio of the mass flow rates of particles and air.

[c]Slip only considered for separated flow predictions. Slip conditions were corrected to an equivalent initial momentum and no slip for LHF model predictions.

Adequate information concerning initial conditions was not available for any of the particle-laden jet experiments. Present estimates of initial conditions for the computations are summarized in Table 2. The jet was formed by relatively short nozzles for the measurements of Yuu et al. [11] and McComb and Salih [21,22]; therefore, the slug flow approximation was employed to specify these initial velocity profiles. Laats and Frishman [23,24] and Levy and Lockwood [25] used relatively long constant diameter tubes for injectors and fully developed pipe flow was taken to be the best approximation for properties at the jet exit. Due to lack of other information, particle concentrations were assumed to be uniform over the jet exit in most cases. The data of Laats and Frishman [23,24] was an exception, they provided the ratio of centerline to average particle mass flux at the jet exit; therefore, simple power law distributions were assumed which yielded this ratio. Yuu et al. [11] and Levy and Lockwood [25] provide sufficient information concerning properties of their particle mixing and injection system so that initial particle velocities could be estimated. A DSF model was used for these calculations. For lack of such details, it was necessary to assume no slip between the phases at the injector exit for the measurements of Refs. [21-24]. Effects of initial particle velocity fluctuations were ignored in the separated flow calculations, but are intrinsically considered in the specification of initial conditions for LHF calculations.

3.2 Model Calibrations

The evaluation of the k-ε turbulence model predictions for constant and variable density single-phase jets is described elsewhere [1,5-7,16]. The data base used for this evaluation included measurements by Shearer et al. [5], Mao et al. [6], Wygnanski and Fiedler [26], Becker et al. [27], Corrsin and Uberoi [28], and Hetsroni and Sokolov [29]. The model generally yielded satisfactory predictions of $\bar{u}$, $\tilde{f}$, k and Reynolds stresses in these flows. Therefore, its use to find mean and turbulent properties of the continuous phase during present calculations is justified, although further improvements could be adopted by the LHF, DSF and SSF models with no fundamental difficulty.

The method for specifying eddy properties and lifetime in the SSF model is somewhat arbitrary. Therefore, the procedure was evaluated using the analytical results of Hinze [18] for dispersion of infinitely small particles injected at a constant rate from a point source in a homogeneous isotropic turbulent flow--similar to Gosman and Ioannides [12]. The calibration results are illustrated in Fig. 1. Stochastic model predictions from Gosman and Ioannides [12] and the present model are shown, along with the exact analytical results from Hinze [18]. The present model is in good agreement with the exact results, indicating satisfactory calibration. The results for the LSSF and NSSF models are the same in this case, since infinitely small particles are always captured by eddies and only the method for

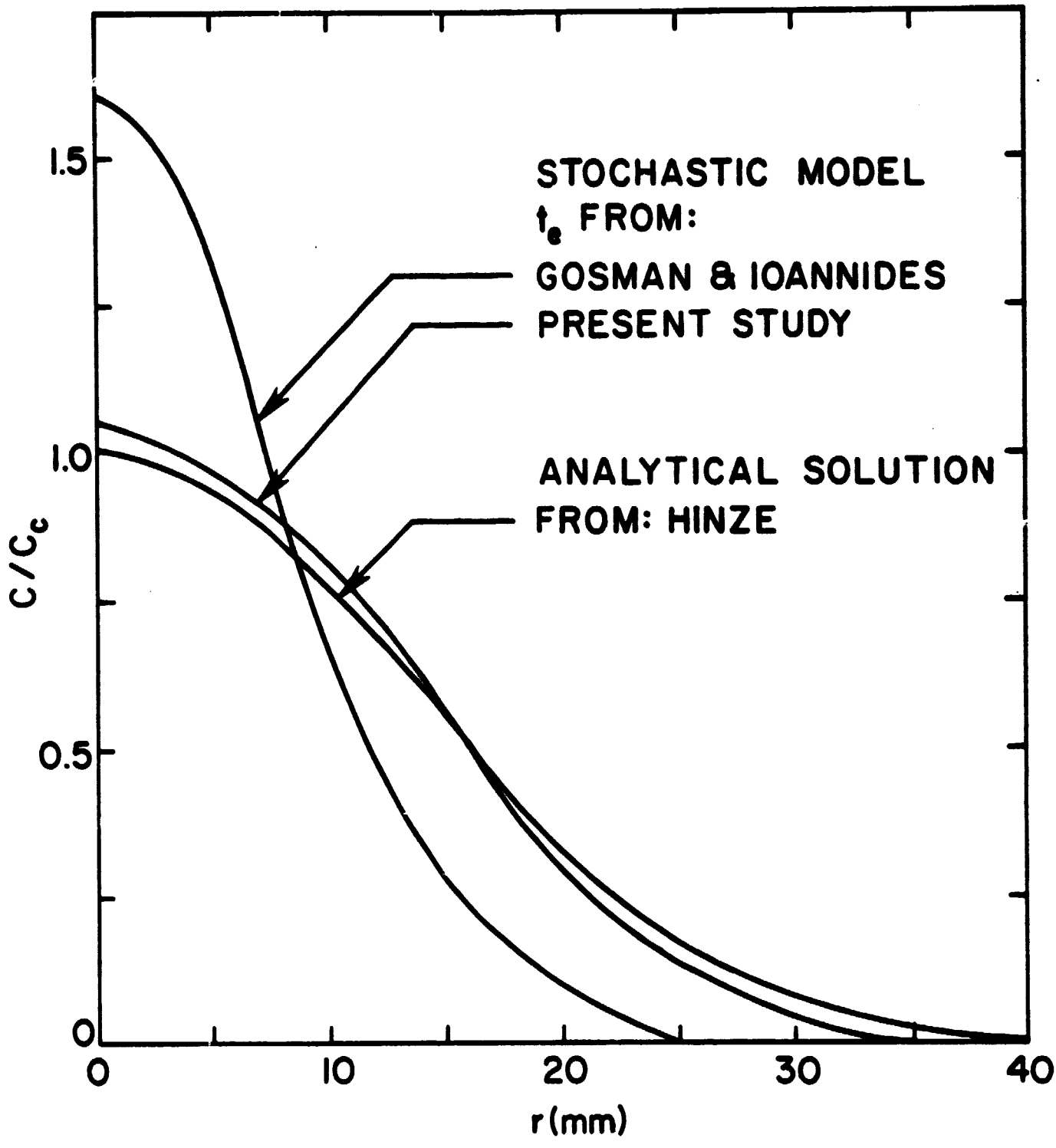

Fig. 1. Analytical and stochastic solutions for the dispersion of small particles in homogeneous isotropic turbulent flow after long diffusion times.

computing eddy lifetime is relevant. The Gosman and Ioannides [12] model, as posed, yields poorer agreement due to a computational error in their original work that has since been corrected [30].

Predictions of the present stochastic LSSF model, as well as the version of Gosman and Ioannides [12] and the measurements of Snyder and Lumley [20] are illustrated in Fig. 2. These experiments involved dispersion of individual particles which were isokinetically injected into a uniform turbulent flow downstream of a grid. The two models yield nearly the same results for heavy particles where the calibration error of [12] has little effect. The present model yields better agreement for the lighter particles where calibration of characteristic eddy time and length scales is more significant since light particles tend to be captured by the eddies. Results for the NSSF model were also compared with this data, these predictions were slightly improved over the LSSF results illustrated in Fig. 2.

3.3 Results and Discussion

Measurements of Yuu et al. [11]. The significance of turbulent particle dispersion in particle-laden jets can be appreciated from the results appearing in Fig. 3. The particle concentration measurements of Yuu et al. [11] are illustrated along with the predictions of the LHF, DSF and NSSF models (NSSF and LSSF model predictions are nearly identical in this case). Predictions are provided for values of x/d which bound the range of the data.

The rate of particle spread is overestimated by the LHF model in Fig. 3, since the particles are predicted to be too responsive to lateral turbulent fluctuations as a result of neglecting slip between the phases. On the other hand, the rate of particle spread is underestimated by the DSF model, since radial particle velocities which contribute to particle spread are only generated by the $\bar{v}$ velocity component--which is small in comparison to radial velocity fluctuations near the axis of jets [26]. The DSF model predictions also indicate that particles are confined to a progressively narrower range of r/x as x/d increases, which is contrary to the measurements. The DSF model yielded poor results for the remainder of the evaluation and will not be considered in subsequent figures for particle-laden jets. In contrast to the relatively poor performance of the LHF and DSF models, the SSF model predictions are in good agreement with the measurements in Fig. 3.

Predictions of the LHF and LSSF models are compared with data from Yuu et al. [11], over a broader range of conditions, in Fig. 4 (the results for u_o = 50 m/s can be compared with Fig. 3 to indicate the differences between LSSF and NSSF predictions). In general, the LSSF model provides good predictions while the LHF model continues to overestimate the rate of particle spread.

Measurements of McComb and Salih [21,22]. The LHF and SSF (both SSF versions yielding nearly the same results) model predictions are

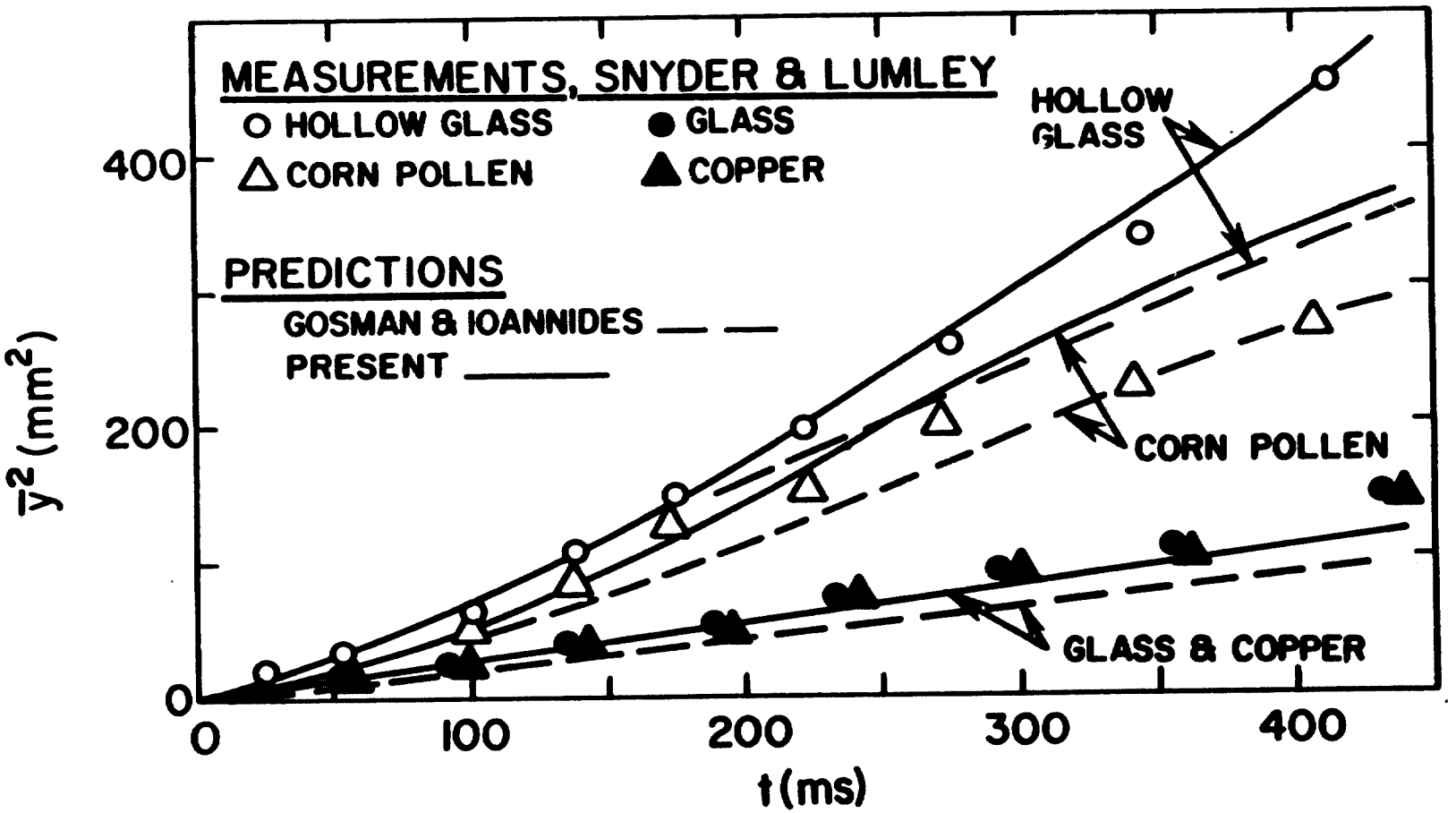

Fig. 2. Predicted and measured particle dispersion in a uniform grid-generated turbulent flow. Data of Snyder and Lumley [20].

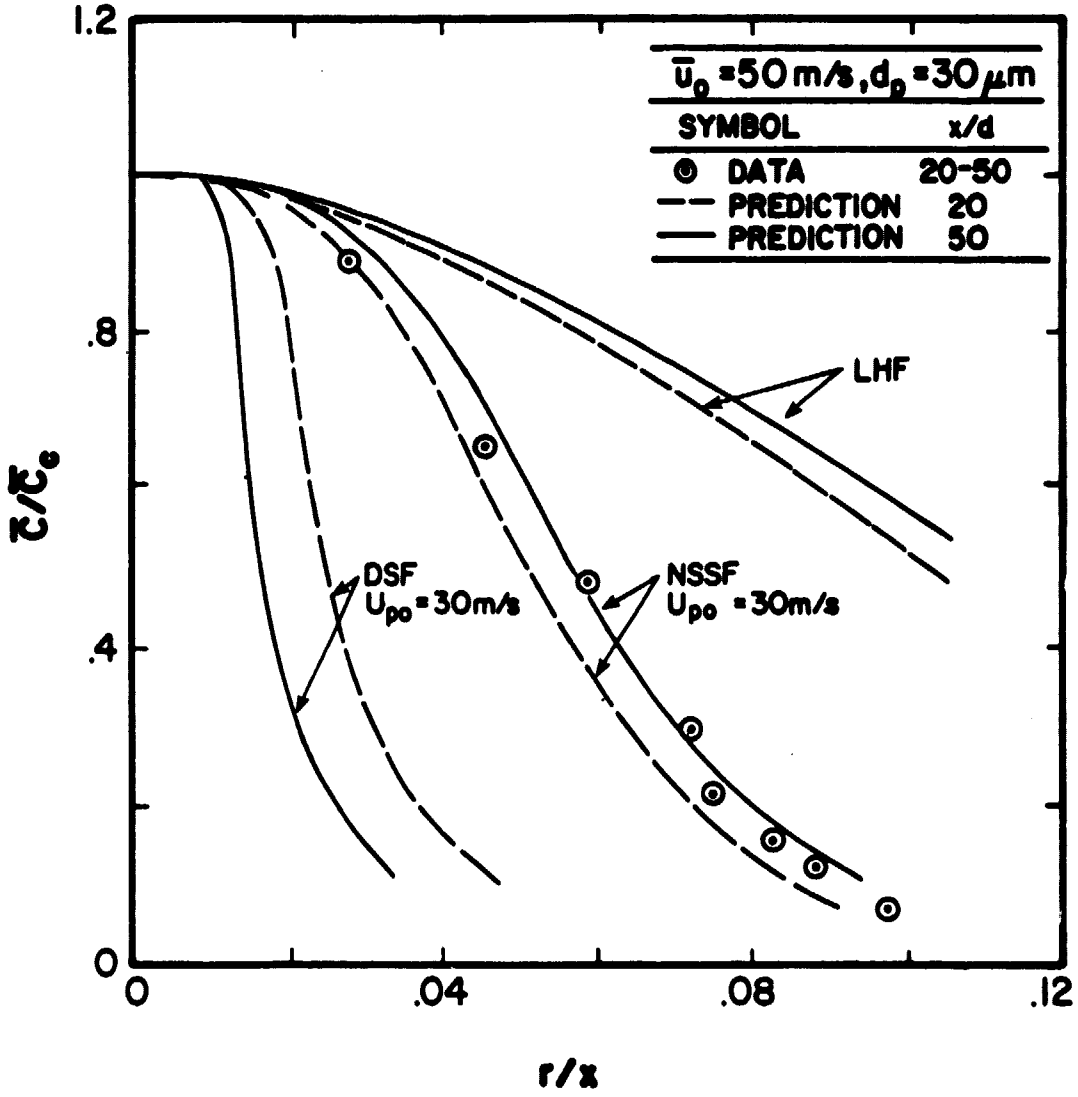

Fig. 3. Comparison of LHF, DSF and NSSF model predictions of particle dispersion in an axisymmetric jet--data of Yuu et al. [11].

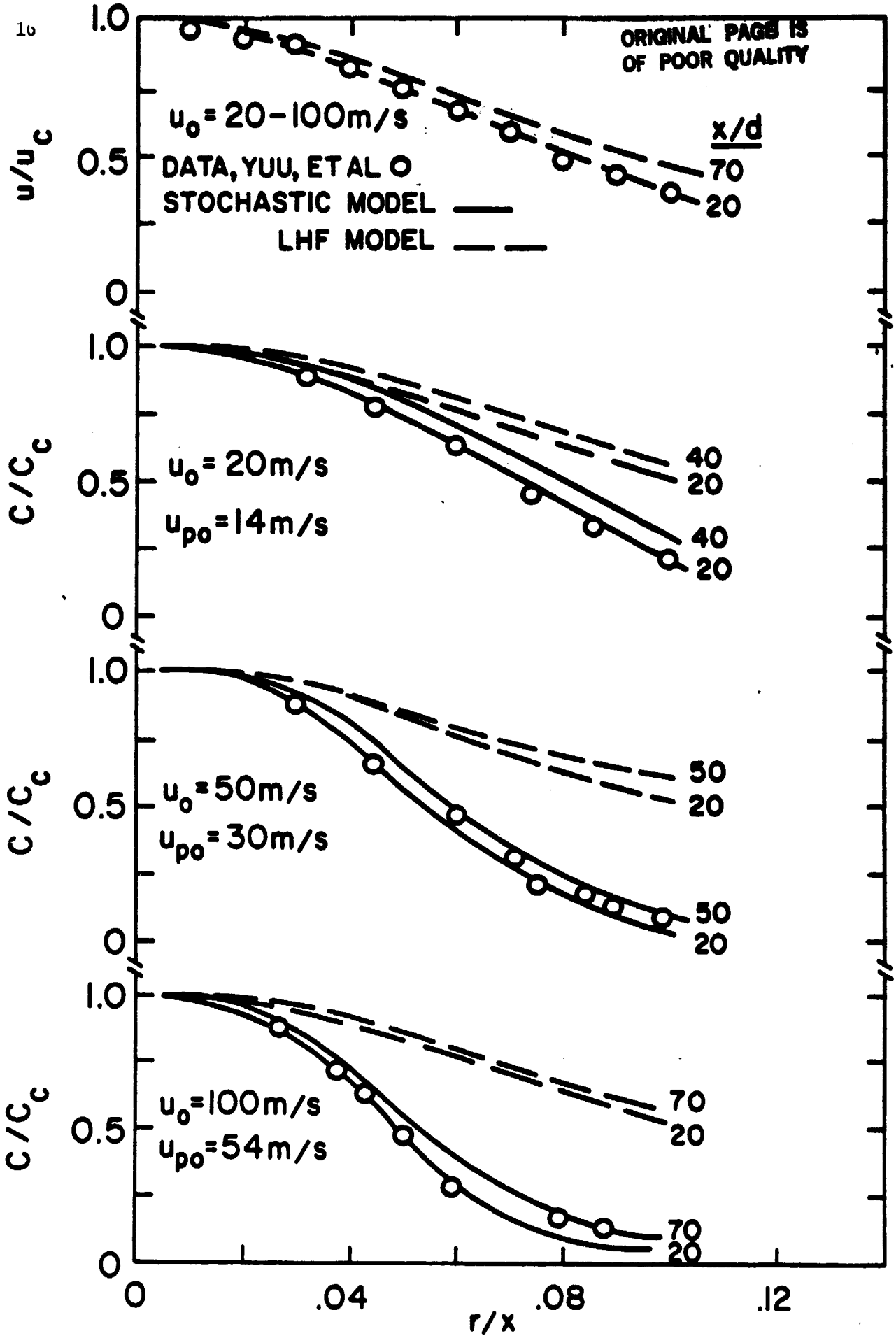

Fig. 4. Predicted and measured axial gas velocities and particle concentrations in a dust-laden jet. Data of Yuu, et al. [11].

compared with the measurements of McComb and Salih [21,22] in Figs. 5 and 6. Results for relatively small titanium dioxide particles, 2.3 μm in diameter, appear in Fig. 5. In this case, these small particles act nearly like tracer particles and the LHF model yields adequate results. The SSF models underestimate particle dispersion slightly, but are also in reasonably good agreement with the measurements.

Results for larger particles, 5.7 μm in diameter, are illustrated in Fig. 6. These particles were tungsten and had a density roughly five times greater than the titanium dioxide particles considered in Fig. 5, cf. Table 2. The greater size and density of the tungsten particles increases their inertia so that effects of slip are more important for the conditions of Fig. 6. In this case, only the SSF models yield adequate agreement with the measurements while the LHF model overestimates both the rate of spread of the particles and the flow.

Results thus far were limited to relatively low particle loadings. This implies that while the gas flow influences particle dispersion, the effect of the particles on the structure of the gas flow was small. This deficiency in the evaluation of the models is rectified by comparison with the measurements of Laats and Frishman [23,24] and Levy and Lockwood [25] in the following. These measurements involved relatively large particle loadings, resulting in significant effects of particles on the structure of the gas phase.

Measurements of Laats and Frishman [23,24]. Particle mass fluxes along the axis were observed to increase for a time near the jet exit for a portion of the data of Laats and Frishman [23,24]. The authors attribute this effect to Magnus forces induced by the particle/gas mixing and injection processes. This effect could not be prescribed sufficiently to include it in the calculations; therefore, data exhibiting such trends are not considered in the following.

Predictions of the NSSF and LSSF models are compared with the measurements in Figs. 7 and 8. Only a range of initial gas velocities were specified for the data; therefore, results are provided for both limits of the velocity range. The predicted effects of initial velocity changes in this range are small, in agreement with observations [23,24].

Predicted and measured mean gas velocities along the jet axis are illustrated in Fig. 7. Results are shown for both particle-laden jets and an air jet. The gas is not strongly influenced by the momentum of the particles at low particle loadings and mean-gas velocities approach the air-jet properties--even for large particles. As particle loading increases, however, the rate of decay of centerline velocity is reduced. This trend is reproduced by the NSSF model, with the LSSF version yielding essentially the same results--except at the highest loading ratios where the models overestimate the rate of flow development.

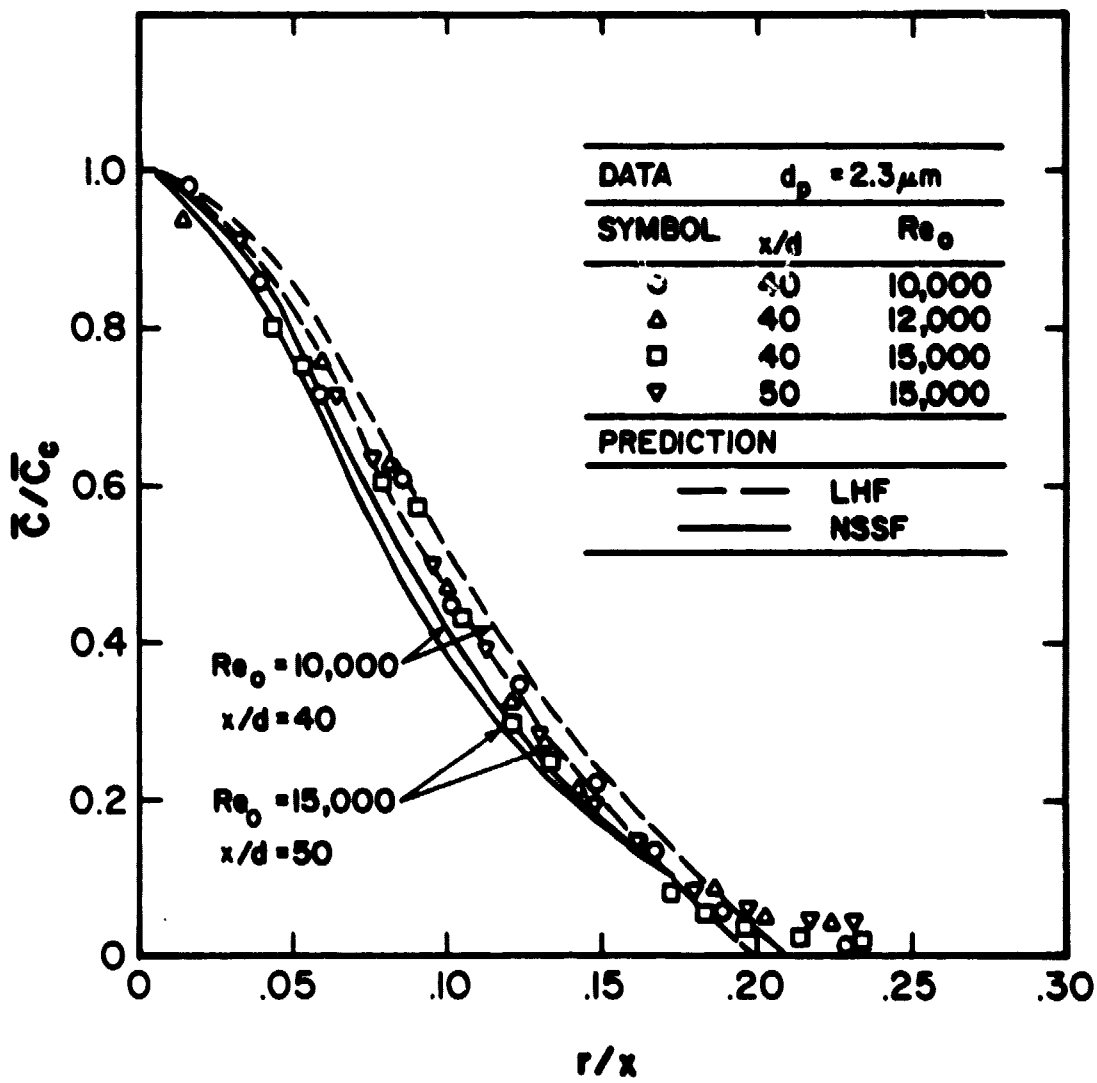

Fig. 5. Predicted and measured particle concentrations in particle-laden jets--data of McComb and Salih [21,22].

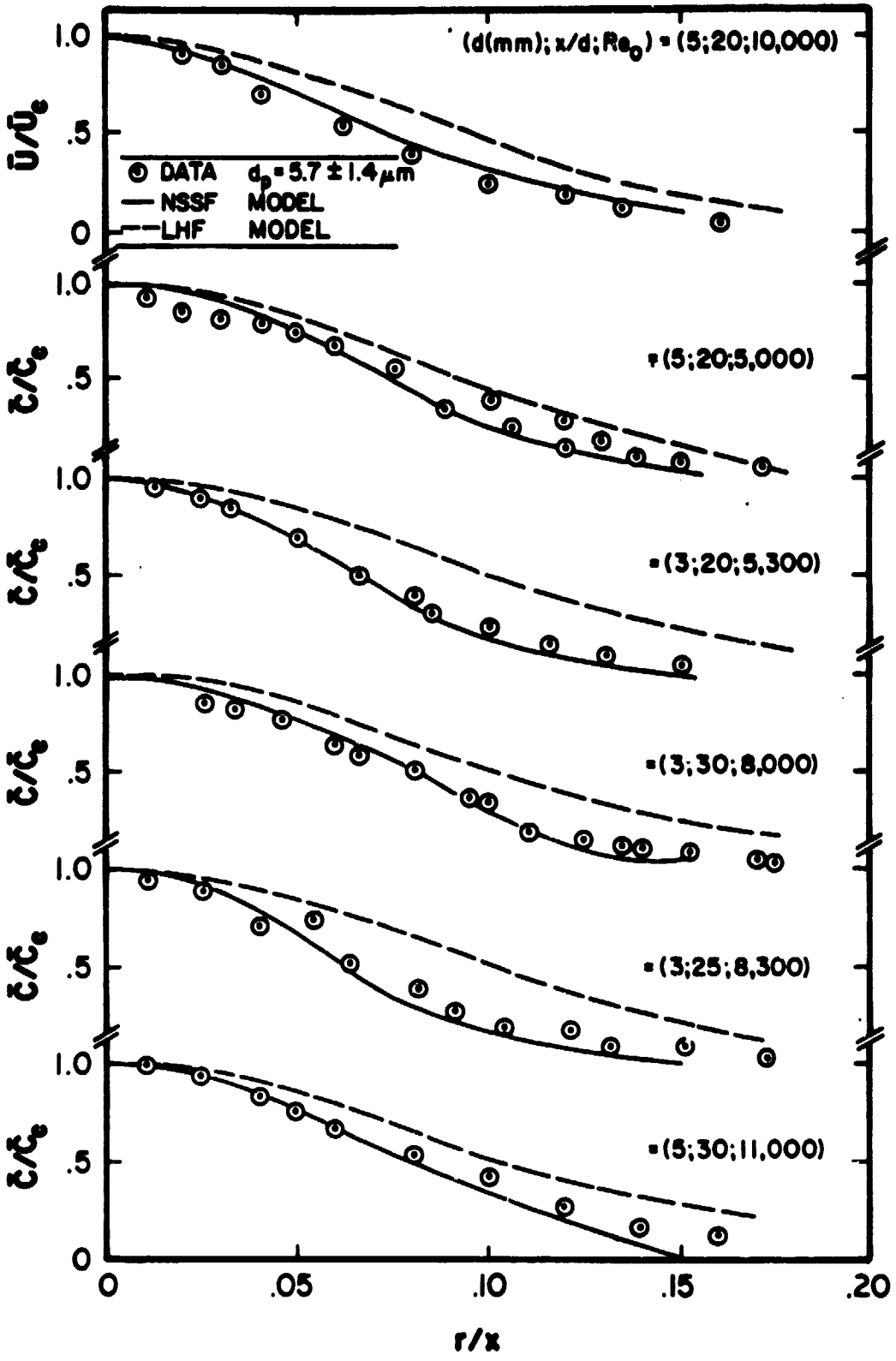

Fig. 6. Predicted and measured axial gas velocities and particle concentrations in particle-laden jets--data of McComb and Salih [21,22].

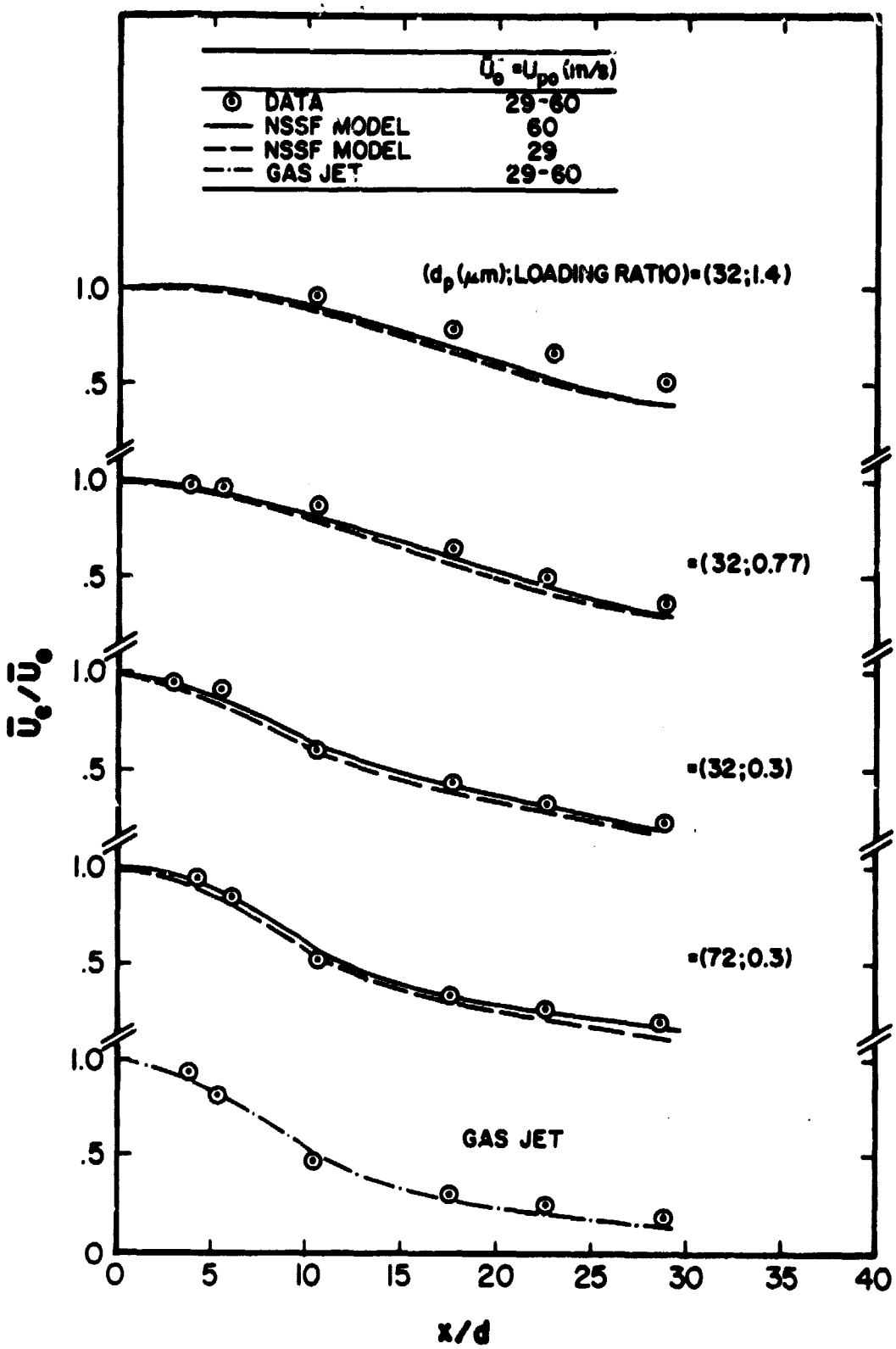

Fig. 7. Predicted and measured axial mean velocities along the centerline of particle-laden jets--data of Laats and Frishman [23,24].

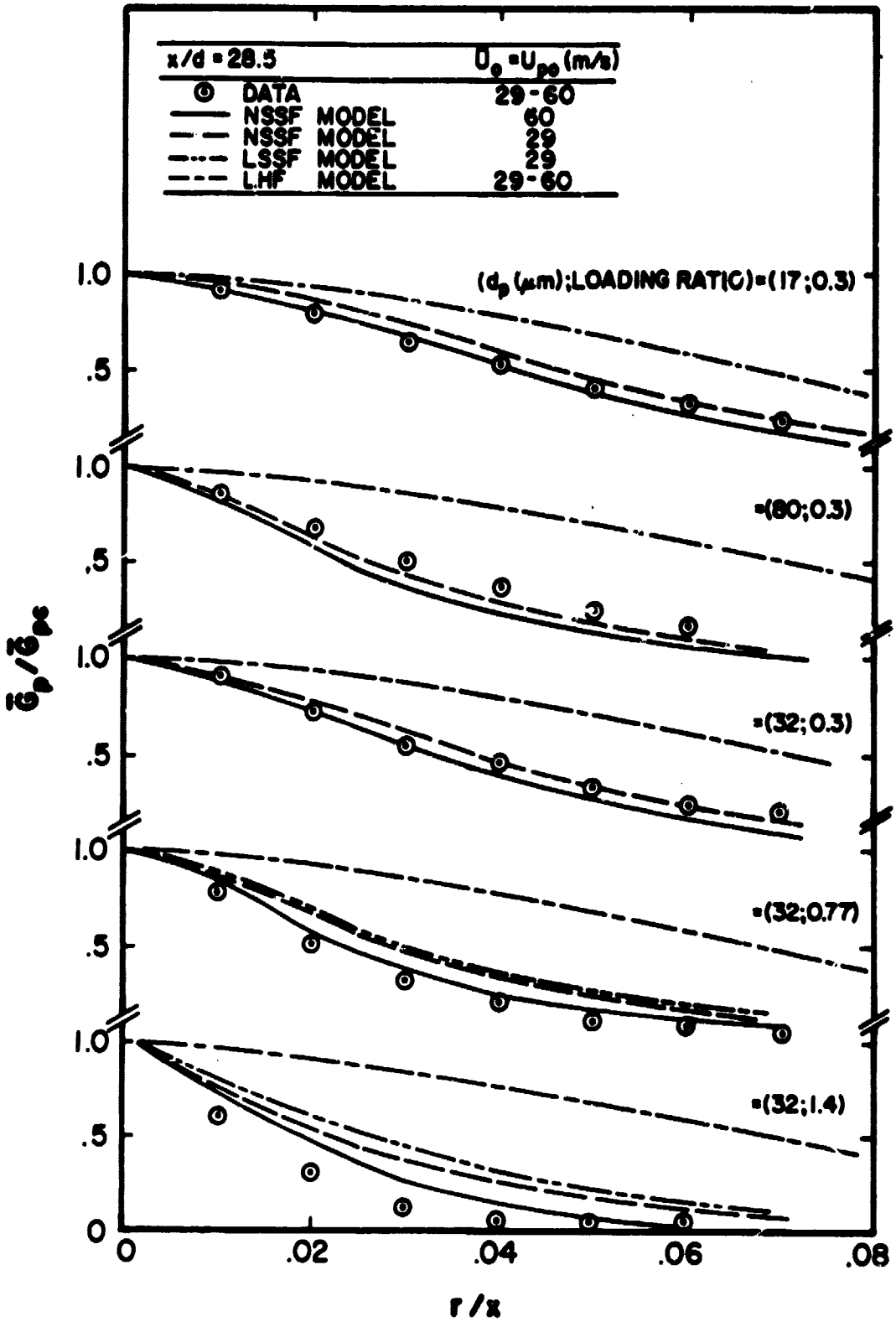

Fig. 8. Predicted and measured particle mass flux in particle-laden jets--data of Laats and Frishman [23,24].

Predicted and measured particle mass flux for various conditions are illustrated in Fig. 8. The results are for x/d = 28.5 since Laats and Frishman suggest that this is beyond the range where Magnus effects were important. The LHF model significantly overestimates the rate of particle dispersion in all cases since the test particles have significant inertia. The SSF models, however, yield reasonably good predictions--particularly the NSSF version--except at the highest particle loadings where the rate of development of the flow is overestimated similar to Fig. 7. Less satisfactory agreement is also observed for the 80 μm diameter particles at a loading ratio of 0.3, where predictions underestimate the rate of particle spread. In this case, initial slip may be a factor since such large particles are less likely to equilibrate in the injector tube, e.g., use of 30% slip at the injector exit yields good agreement between predictions and measurements.

Two effects may be responsible for the poorer performance of the SSF models at higher loading ratios, seen in Figs. 7 and 8. The effect of Magnus forces, discussed earlier, causes particles to be deflected toward the centerline of the flow in a manner not considered in the analysis. This would reduce rates of apparent turbulent particle dispersion and would also feed additional momentum from the deflected particles to the flow near the centerline--tending to reduce rates of axial velocity decay. A second effect could be the turbulence modulation phenomena discussed by Al Taweel and Landau [31]. This effect involves damping of turbulent fluctuations by the drag of the particles. Lower turbulence levels reduce rates of particle spread by turbulent dispersion as well as the turbulent mixing of the continuous phase, which would also explain why the SSF models overestimate rates of flow development at high loading ratios. Unfortunately, information available is not sufficient to evaluate the relative significance of these two effects. The unusual properties of the measurements of Refs. [23,24] even at moderate particle loadings, however, cannot be attributed to turbulence modulation. This suggests that Magnus forces may be a major contributor to the difficulty.

Measurements of Levy and Lockwood [25]. Predictions of the NSSF model (LSSF model predictions are nearly the same) and the measurements of Levy and Lockwood [25] are illustrated in Figs. 9 and 10. LHF model predictions for these flows overestimated rates of flow development similar to results discussed earlier and are not shown on the figures. Predictions of fluctuating gas velocities were obtained using the assumption of isotropic turbulence $\bar{u}'^2 = 2k/3$.

Both predictions and measurements indicate relatively small effects of particle size and loading on gas flow properties in Fig. 9. This is due to the fact that large particle loadings correspond to large particles for these data. Therefore, momentum exchange between the phases was relatively small for the limited axial distance considered during these experiments. Predictions are in reasonably good agreement with measurements, except for the highest particle loading, where measured turbulence intensities are underestimated by the theory.

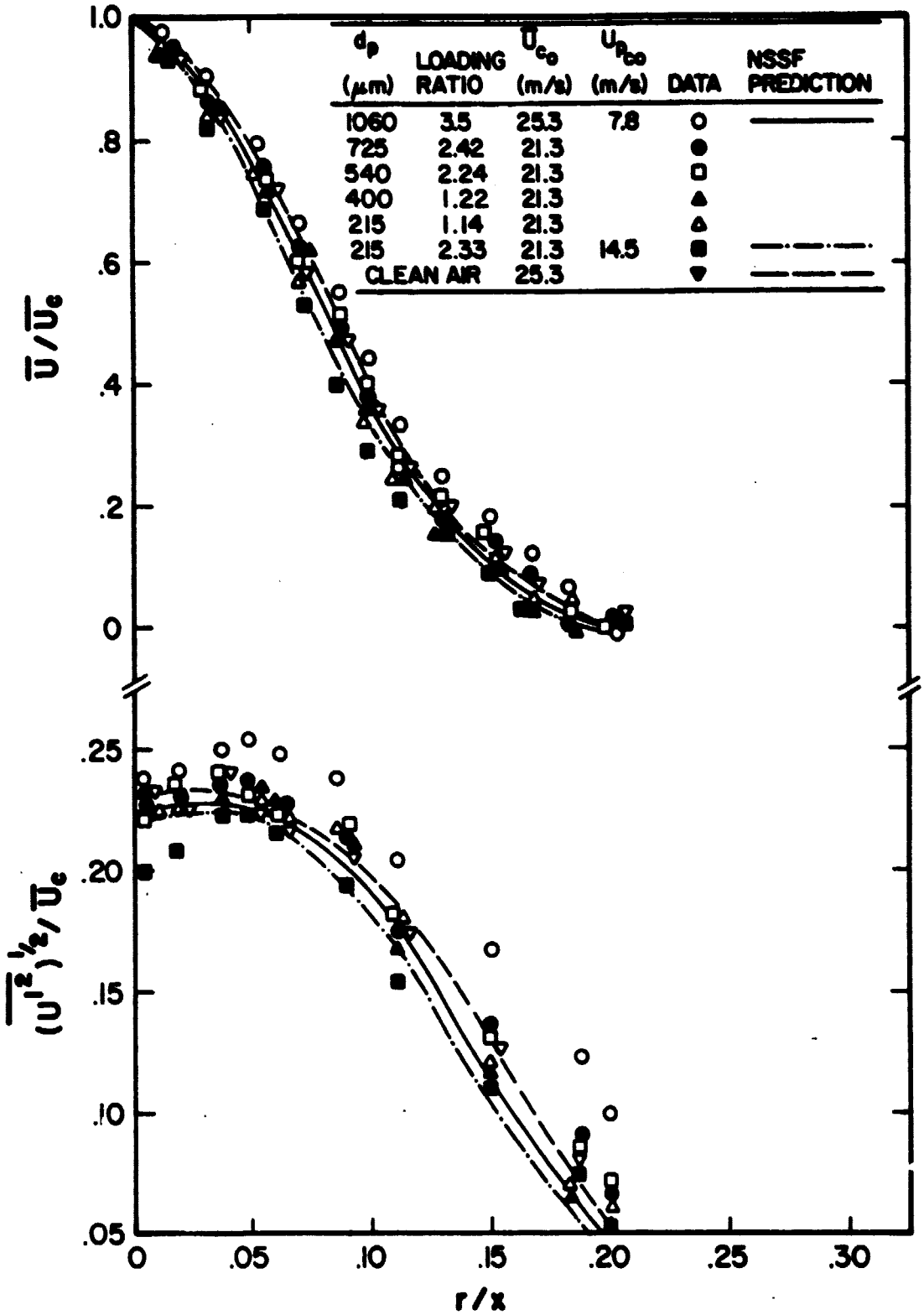

Fig. 9. Predicted and measured mean and fluctuating gas velocities in particle-laden jets--data of Levy and Lockwood [25].

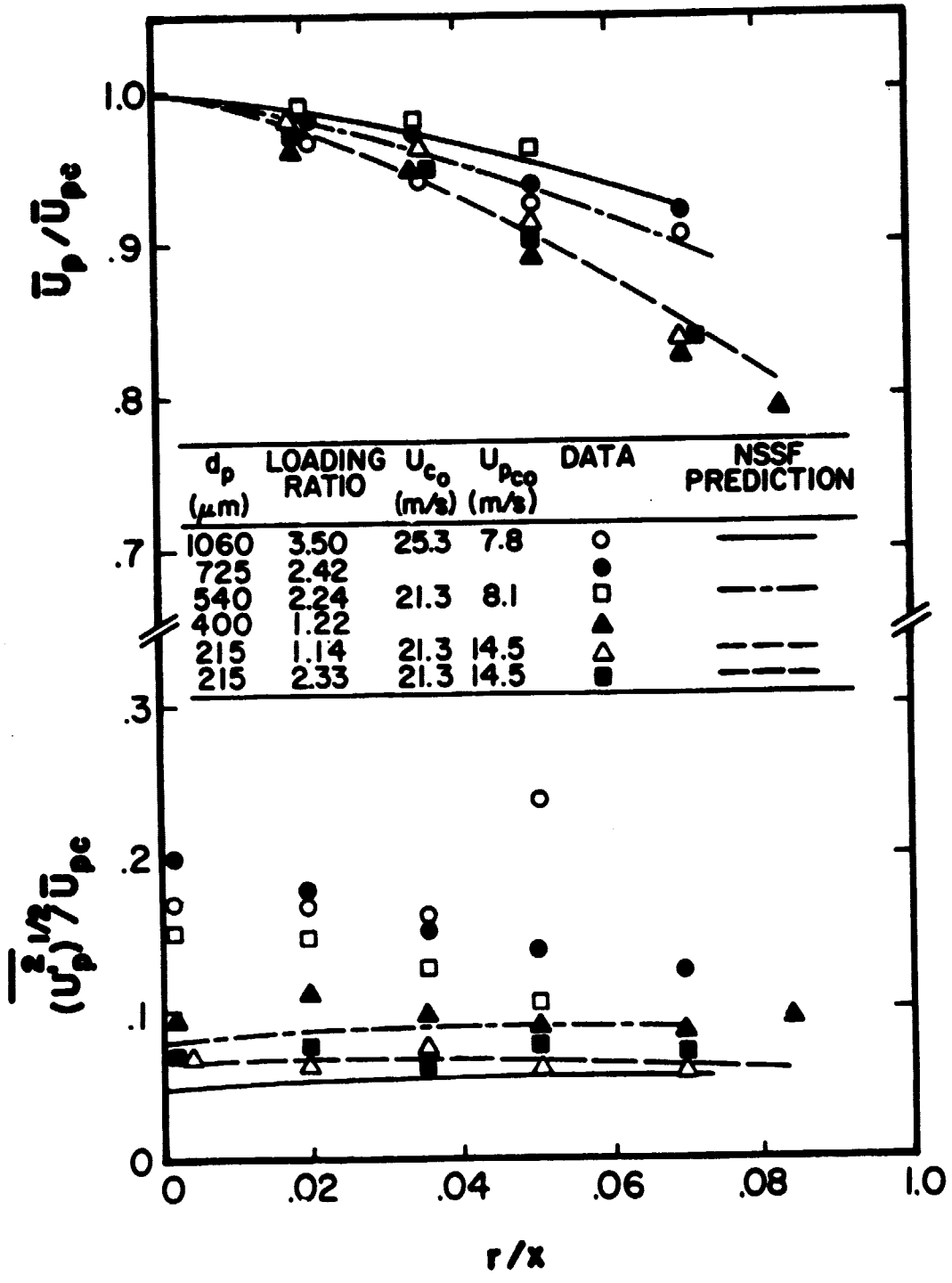

Fig. 10. Predicted and measured mean and fluctuating particle velocities in particle-laden jets--data of Levy and Lockwood [25].

Predicted and measured mean and fluctuating particle velocities are illustrated in Fig. 10. Predictions of mean particle velocities are in good agreement with the measurements at all conditions. Predictions of particle fluctuations, however, are underestimated except for the smallest particles in the data base. This discrepancy increases with the size of the particles, but is not influenced very much by the particle loading ratio.

The progressive underestimation of particle fluctuations with increasing particle size can best be explained as artifact of the particle/gas mixing and injection system (which was a worm-gear drive followed by a relatively short length of ducting). During these tests, the large particles have a relatively small velocity change as they pass from the jet exit to the measuring station, so that they would tend to maintain fluctuation levels which are similar to those at the jet exit. In contrast, the small particles interact with the flow field to a greater degree, so that effects of the injection system are damped out. Since present calculations ignore initial particle fluctuations, results are most satisfactory for small particles where effects of initial conditions are less persistent. Particle velocity fluctuations at the jet exit could also be responsible for the somewhat larger velocity fluctuation levels observed for large particles in Fig. 9.

Another explanation for the larger particle and gas velocity fluctuations observed for large particles could be that the larger slip of these particles enhances turbulent fluctuations in a manner that is not considered in the model. Additional data, including complete specification of particle and gas properties at the jet exit, are needed to clarify the relative importance of turbulence enhancement/modulation and initial condition effects for these data.

In fact, the present evaluation of the DSF and SSF models was inhibited throughout by insufficient information concerning initial conditions. Until these initial condition difficulties are resolved by new experiments, decisive evaluation of turbulent particle dispersion models cannot be completed.

4. SPRAY MEASUREMENTS

4.1 Test Apparatus

Figure 11 is a sketch of the apparatus and major instrumentation for the nonevaporating spray experiments. An air-atomizing injector, cf. Table 3 for specifications, was mounted at the top of a screened enclosure (1 m square and 2.5 m high) to reduce room disturbances. All optical instrumentation was mounted rigidly. Therefore, the injector was traversed to obtain profiles of flow quantities (two directions using the injector mount and the third major traverse by moving the entire screened enclosure). The inlet of the exhaust system was screened and located 1 m below the plane of the measurements. Tests showed that operation of the exhaust system had negligible effect on flow properties at the measuring locations.

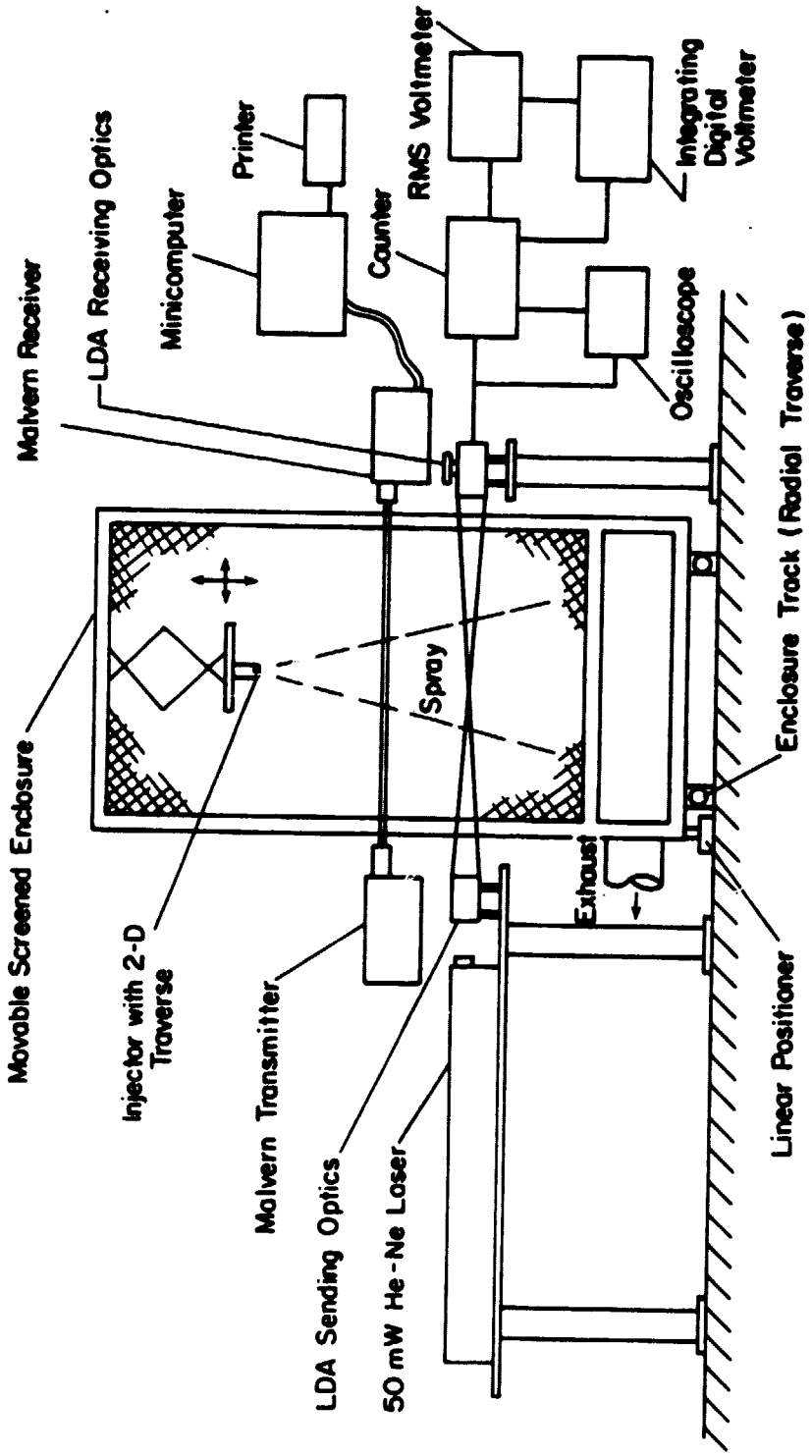

Fig. 11. Sketch of the spray apparatus.

Table 3 Summary of Test Conditions for Nonevaporating Sprays

	Air Jet	Sprays	
		Case 1	Case 2
Injected fluid	air	air and oil[b]	air and oil[b]
Injector flow rates, mg/s			
Gas	338	338	216
Liquid	0	600	1400
Loading ratio[c]	0	1.78	6.48
Jet momentum, mN	120.1	137.2	70.1
Initial velocity, m/s[d]	175	146	43.4
Reynolds number[d]	2.6×10^4	3.0×10^4	2.4×10^4
SMD, μm[e]	0	30	87
Spray angle[f]	-	30	33

[a]All flows employ Spraying Systems air-atomizing injector (Model 1/4J2050 nozzle, No. 67147 air nozzle, 1.194 mm injector exit diameter). Ambient and injector inlet temperature 300 ± 1 K, ambient pressure, 97 kPa.

[b]Sargent-Welch Scientic Co., Duo Seal Oil, Cat. No. 1407K25, density = 878 kg/m^3, vapor pressure at 38°C = 4×10^{-4} mm Hg.

[c]Ratio of injected liquid to gas flow rates.

[d]Assuming LHF. The viscosity of air was employed for the Reynolds number.

[e]Measured with the Malvern, Model 3300 Particle Sizer at x/d = 12.6.

[f]Determined from liquid flux measurements, cf. Section 4.2.

The injector flow system is illustrated in Fig. 12. Filtered dry air is supplied from a storage tank. The flow rate of air is controlled with a pressure regulator and metered with a critical-flow orifice to insure stable long-term operation. The liquid is stored in a tank under pressure, however, the tank is not agitated and pressure levels are moderate (0.3-0.8 MPa). Therefore, the dissolved air content of the liquid is negligible. The flow rate of liquid is controlled with a valve and metered with a rotameter. In order to maintain repeatable flow and atomization conditions the entire test cell is heated above normal ambient temperatures--to 27 $\pm 1^{\circ}$C.

The spray liquid was vacuum-pump oil. This precluded significant evaporation in the flow field--even when finely atomized--due to low liquid volatility, cf. Table 3.

4.2 Instrumentation

A single-channel, frequency-shifted LDA was used for measurements of mean and fluctuating gas velocities. Several beam orientations provided measurements of all velocity components as well as the Reynolds stress. Concentration biasing and effects of drops were avoided by employing high concentrations of seeding particles (0.2 μm diameter), similar to past work [5]. Data densities were high, allowing analog processing to obtain time-averaged quantities.

Injector operation was monitored continuously by measuring drop sizes with a Malvern Model 3300 particle sizer. This instrument operates on the principle of Fraunhofer diffraction of laser light. The measuring region of the instrument included the entire spray width, centered at $x/d = 12.6$, with the input laser beam having a diameter of 9 mm. Injector properties were also monitored by periodically measuring injector thrust with an impact plate [5]. Spray angles were found from liquid flux measurements (taken as the angle from the injector exit which bounds the region where the liquid mass flux is greater than 1% of its centerline value at $x/d = 50$).

Profiles of drop-size distributions were measured by a slide impactor, developed earlier [5]. The samples measured on the slide were corrected for the collection efficiency of the probe, using a correlation due to Ranz, cf. Ref. [5] and references cited therein for a description of this correction. Depending on the spray condition, 500-3000 drops were measured to establish statistically significant drop-size distributions.

Liquid fluxes were measured with an isokinetic sampling probe. The probe had a 3 mm ID sampling port, followed by a gas-flushed diverging section which prevented premature drop impaction on probe surfaces. The drops were captured on a filter, which was weighed after a timed period of collection to determine liquid fluxes. Mass conservation checks of liquid flow rates were satisfied within 15% for the measurements reported here.

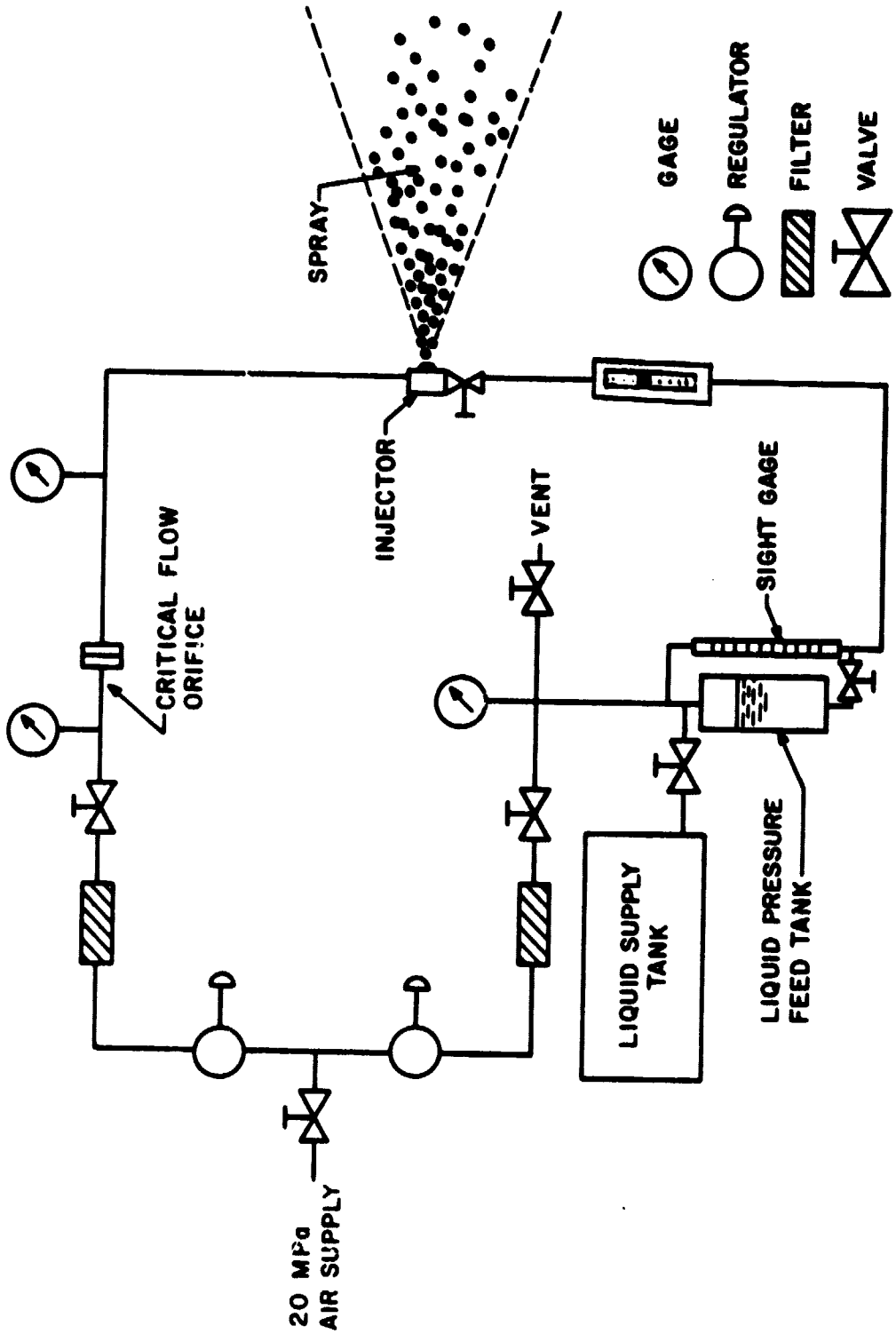

Fig. 12. Sketch of the injector flow system.

4.3 Test Conditions

Three test conditions were considered: (1) a pure air jet, formed by the injector, to serve as a baseline; (2) a spray having a nominal Sauter mean diameter (SMD) of 30 μm, similar to the spray considered in Ref. [5]; and (3) a spray having a SMD of 87 μm, which exhibits significant effects of slip. The properties of these three test conditions are summarized in Table 3.

5. MODEL EVALUATION: SPRAYS

5.1 Air Jet Calibration

The measurements of mean and fluctuating velocities in the air jet were in good agreement with earlier measurements by Shearer et al. [5] using a similar twin-fluid injector. The comparison between predictions and measurements was also satisfactory--similar to Ref. [5]. This established an acceptable baseline for measurements in the sprays and these results will not be considered any further here.

5.2 Initial Conditions

Due to its small size, measurements at the exit of the injector were limited to mass flow rate and momentum of the two-phase jet. The latter measurement was completed using an impact plate, similar to Ref. [5].

Photographs of the two sprays appear in Figs. 13 and 14. Determination of spray angles from photographs is a subjective matter, also influenced by the lighting, film and exposure of the film. The values found from present photographs for case 1 and 2 sprays are 24^{o} and 21^{o}. These values are less than the angles found from the liquid flux measurements--which provide far greater sensitivity for determining the presence of liquid.

Due to limitations of spatial resolution, profiles of spray properties were only measured at $x/d \geq 50$. In particular, detailed measurements of drop-size distributions , liquid flux, and mean and fluctuating gas velocities were undertaken at $x/d = 50$, in order to define initial conditions for the SF computations.

Drop size distributions for various radial positions at $x/d = 50$ for the two sprays are illustrated in Fig. 15. Although the distributions differ in detail at the various radial locations, the SMD is relatively uniform across both sprays, cf. Fig. 15. The values of the SMD at this axial station are larger than the nominal size obtained by the Fraunhofer diffraction measurements, since: (1) this position is farther from the injector which allows drop sizes to increase by collisions and coalescence in the dense portion of the spray; (2) the slide impactor has reduced collection efficiencies for small drops [5], which tends to bias its measurement toward larger

Fig. 13. Photograph of the case 1 spray.

Fig. 14. Photograph of the case 2 spray.

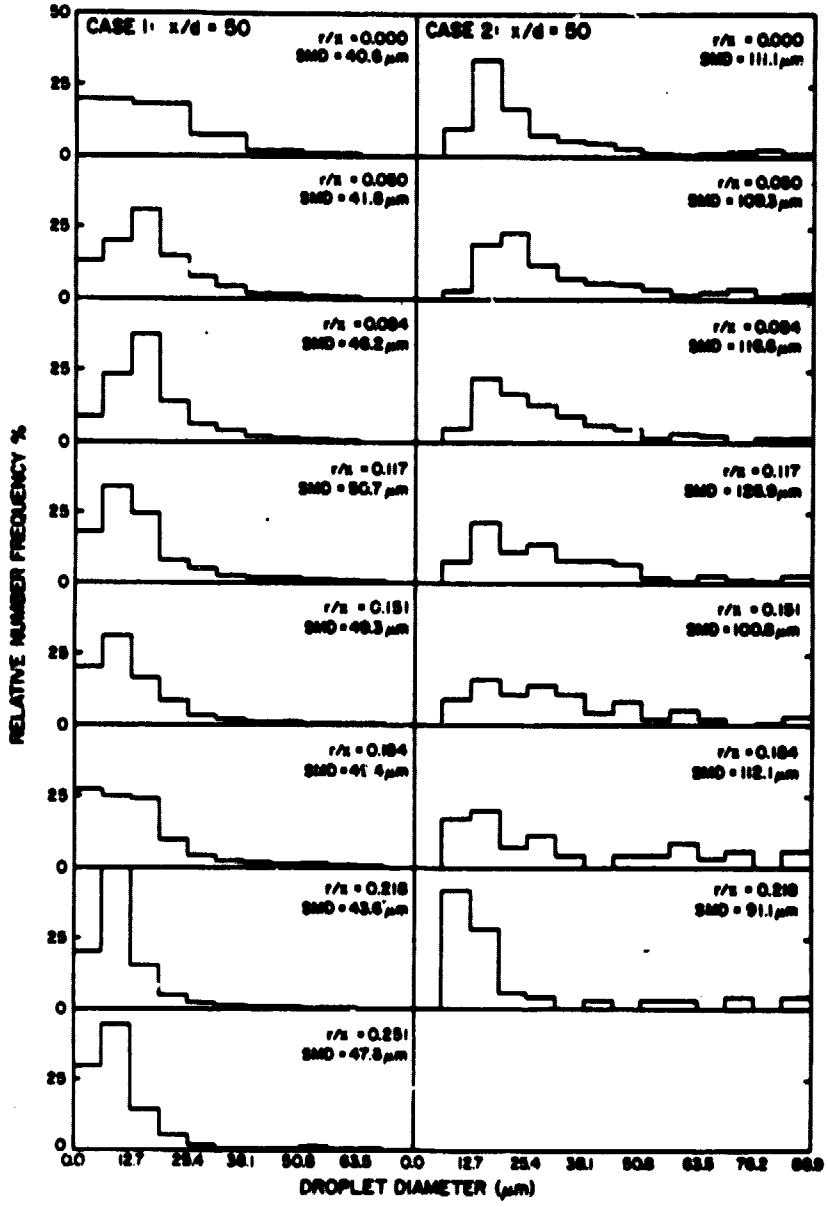

Fig. 15. Drop size distributions for the nonevaporating sprays at x/d = 50.

drop sizes even after correction; and (3) the slide impactor is more effective for finding occasional large drops than the Fraunhofer diffraction method, which also tends to increase the SMD measured by impaction.

The SMD measurements illustrated in Fig. 16 indicate that drops are observed for $r/x > 0.2$, which is beyond the edge of most fully-developed, single-phase jets. This effect is attributable to both initial radial velocities produced at the injector and dispersion of drops by turbulent fluctuations. Further implications of this observation and other measurements at the initial condition ($x/d = 50$) will be considered later.

5.3 Results and Discussion

Once initial conditions were established, the remaining measurements were used to evaluate model predictions. Since the LHF model was not limited to a dilute spray and had appropriate initial conditions at the injector exit, results for this model were obtained throughout the entire flow. The DSF and SSF model predictions, however, were limited to the dilute portion of the spray--beginning at $x/d = 50$ where initial conditions for these models were measured.

Predicted and measured mean gas velocities along the axis of the two sprays are illustrated in Fig. 17. The LHF predictions of mean velocity for the more finely atomized spray tend to underestimate the measurements slightly, similar to the findings of Shearer et al. [5] for an evaporating spray having a similar SMD. It will become evident, however, that this agreement is partly fortuitous, since the LHF model significantly underestimates the width of this spray. Typical of earlier experience with LHF models of sprays [5] the LHF model overestimates the decay of axial velocity in the coarser spray, due to the neglect of effects of slip between the phases. In contrast, the SSF model provides satisfactory predictions of mean centerline velocities for both sprays.

The same models are compared with measurements of liquid mass flux along the axis of the two sprays in Fig. 18. The LHF models do not approach the measurements until large values of x/d, where effects of interphase slip are relatively small. The SSF model, however, provides reasonably good predictions throughout the range of x/d where it was used.

Predicted and measured radial profiles of mean axial gas velocities are illustrated in Fig. 19, including the initial condition, $x/d = 50$. Predictions from both the LHF and SSF models are shown on the plot. The results illustrate an interesting property of these sprays. During the computations for particle-laden jets, the LHF model invariably overestimated the width of the flow since neglecting slip causes the rate of dispersion of heavy particles by the turbulence to be overestimated. In the present case, however, the spray spreads more rapidly than the LHF prediction, due to enhanced dispersion of drops. The increased response of the drops in the present

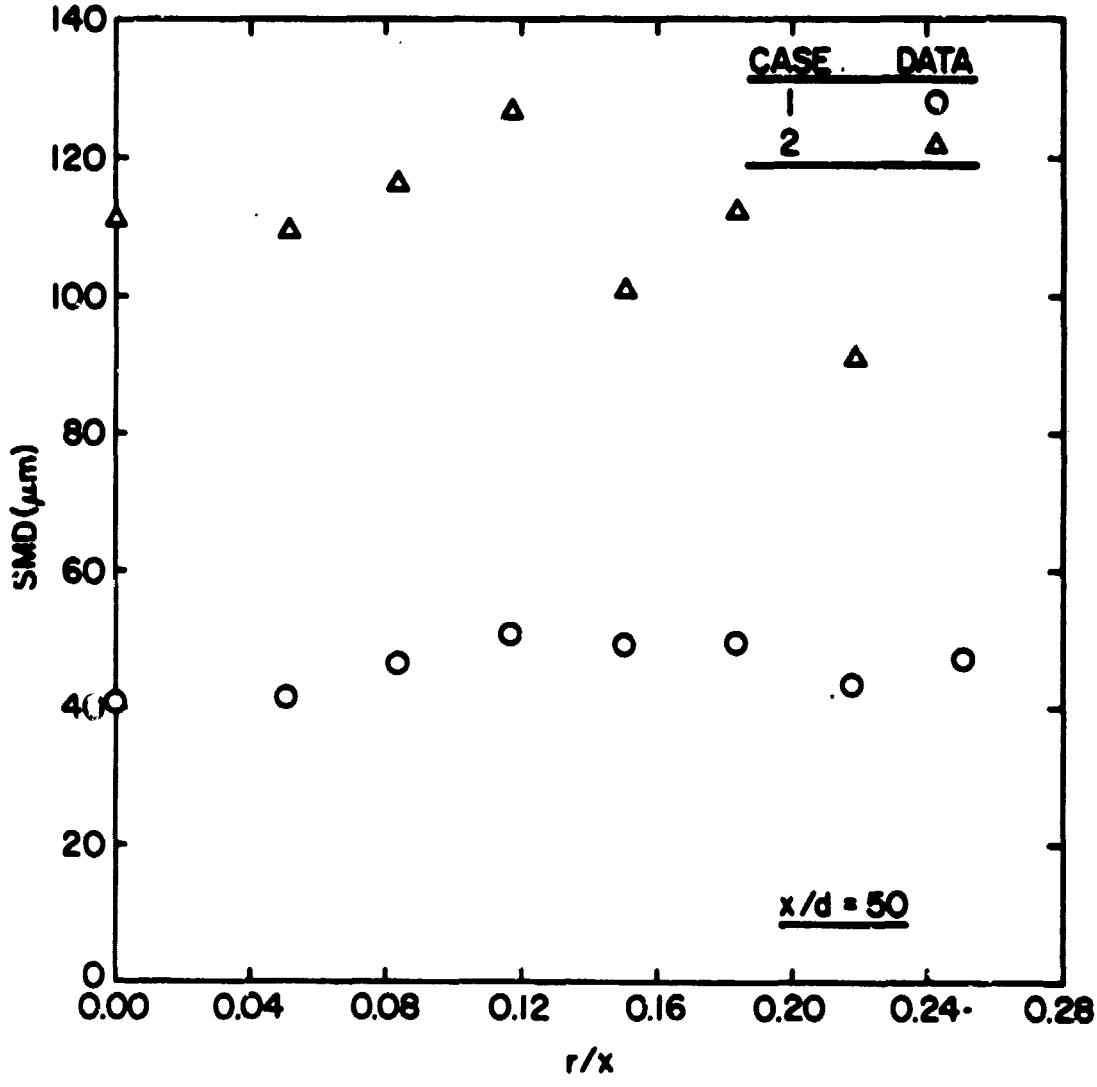

Fig. 16. Radial variation of SMD in the nonevaporating sprays at x/d = 50.

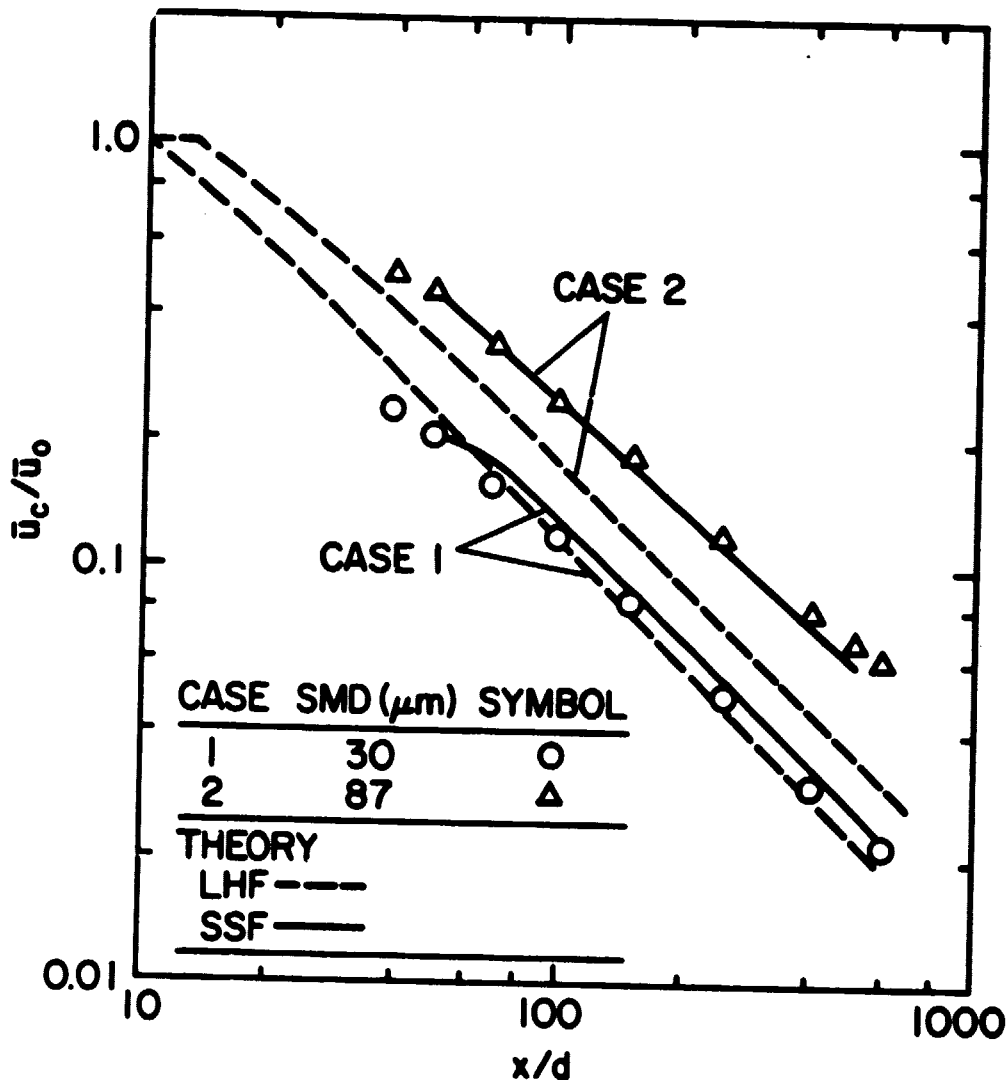

Fig. 17. Predicted and measured mean gas-phase velocities along the axis of the nonevaporating sprays.

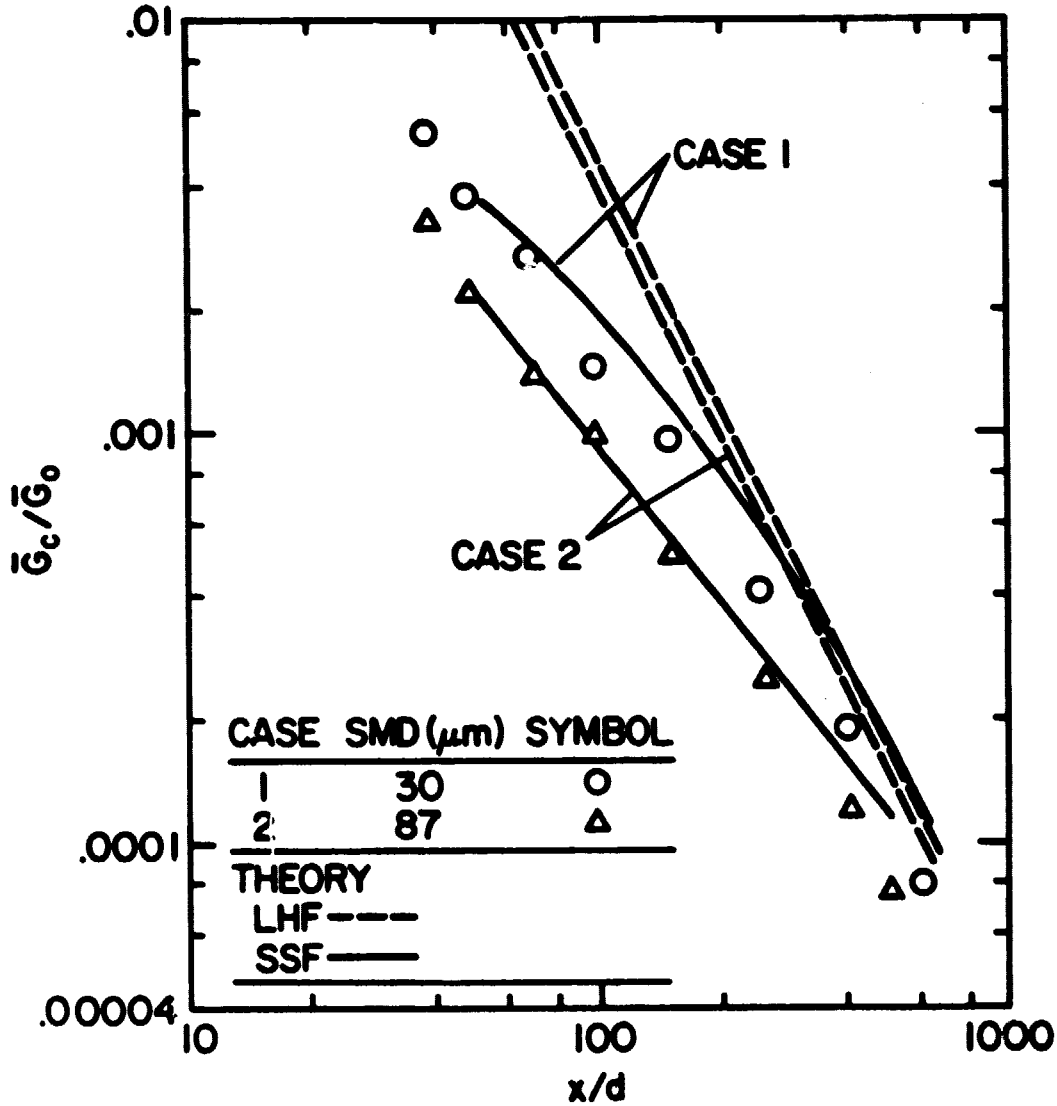

Fig. 18. Predicted and measured mean liquid flux along the axis of the nonevaporating sprays.

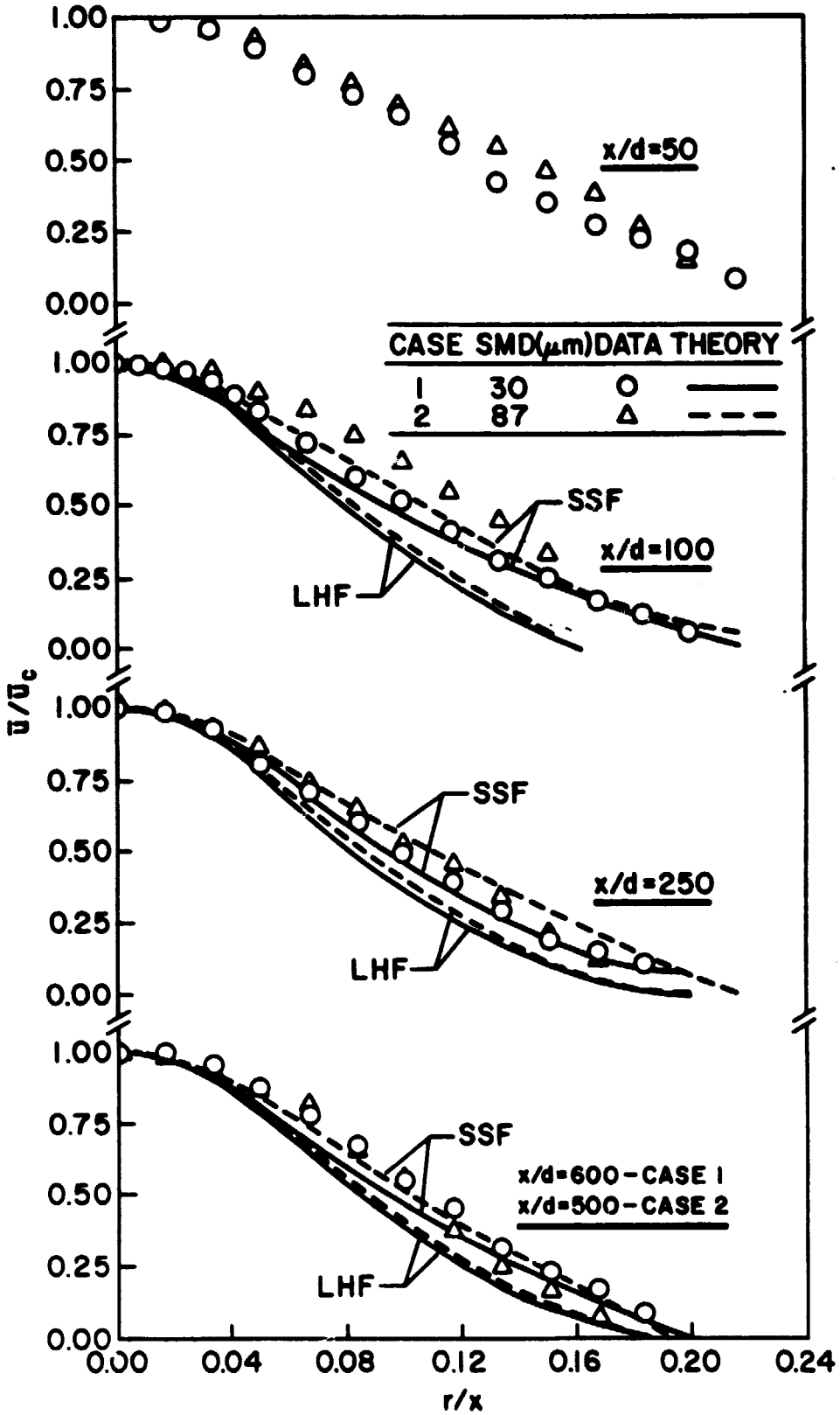

Fig. 19. Predicted and measured radial variation of mean-gas velocity in the nonevaporating sprays.

sprays, in comparison to the solid particles in the particle-laden jets can be attributed to: (1) the smaller density of the drops; (2) the greater rates of flow deceleration due to the smaller injector dimensions of the sprays; and (3) the larger initial slip between the liquid and gas phases in the sprays. It is very encouraging that the SSF model can reproduce this unexpected effect, with no change in the modeling procedure and empirical constants.

Predicted and measured radial profiles of liquid mass flux are illustrated in Fig. 20. In this case, results for the DSF model are shown along with the LHF and SSF predictions. The DSF model yields poor results, similar to particle-laden jets. Neglecting drop dispersion by the turbulence causes the rate of spread of the flow to be substantially underestimated--even after allowing for the apparent radial velocity of the drops at x/d = 50. Other predictions of the DSF model were also not very satisfactory; therefore, this method will not be considered any further here.

As before, the SSF model yields the most satisfactory predictions of flow properties for the results illustrated in Fig. 20. The performance of the SSF model, however, is poorer for liquid flux than for other measurements considered during this study. Since liquid flux predictions are more sensitive to estimations of initial conditions than other spray properties, uncertainties in initial conditions are a potential source for these errors. Additional measurements of drop sizes and velocity will be required to resolve this effect.

All three components of the velocity fluctuations were measured, allowing k to be computed for comparison with predictions. These results are illustrated in Fig. 21. The agreement between predictions of the SSF model and the measurements is reasonably good. The fact that turbulence levels roughly correspond to values estimated from a model which ignores effects of particle motion on turbulence properties, indicates that effects of turbulence modulation (suggested by Al Taweel and Landau [31]) or turbulence production by drops were small for the present flows. This is reasonable, since the comparison is confined to dilute portions of the spray.

Predicted and measured profiles of Reynolds stress are illustreated in Fig. 22. The SSF predictions are adequate for both sprays. This is consistent with the reasonably good predictions of mean velocities and k obtained with this model for the test sprays.

Effects of the presence of drops on turbulence properties are more evident when individual components of velocity fluctuations are examined. Measured radial profiles of u', v' and w' are illustrated in Figs. 23 and 24 for the finely and coarsely atomized sprays. Predictions were obtained assuming $(\bar{u}'^2:\bar{v}'^2;\bar{w}'^2) = (1:0.5:0.5)\ k$, which is approximately observed in the fully-developed region of single-phase round jets [26,32]. Predictions constructed in this manner are in fair agreement with the measurements--particularly in the region far from the injector. A notable feature of the results, however, is that levels of anisotropy are rather high for positions near the

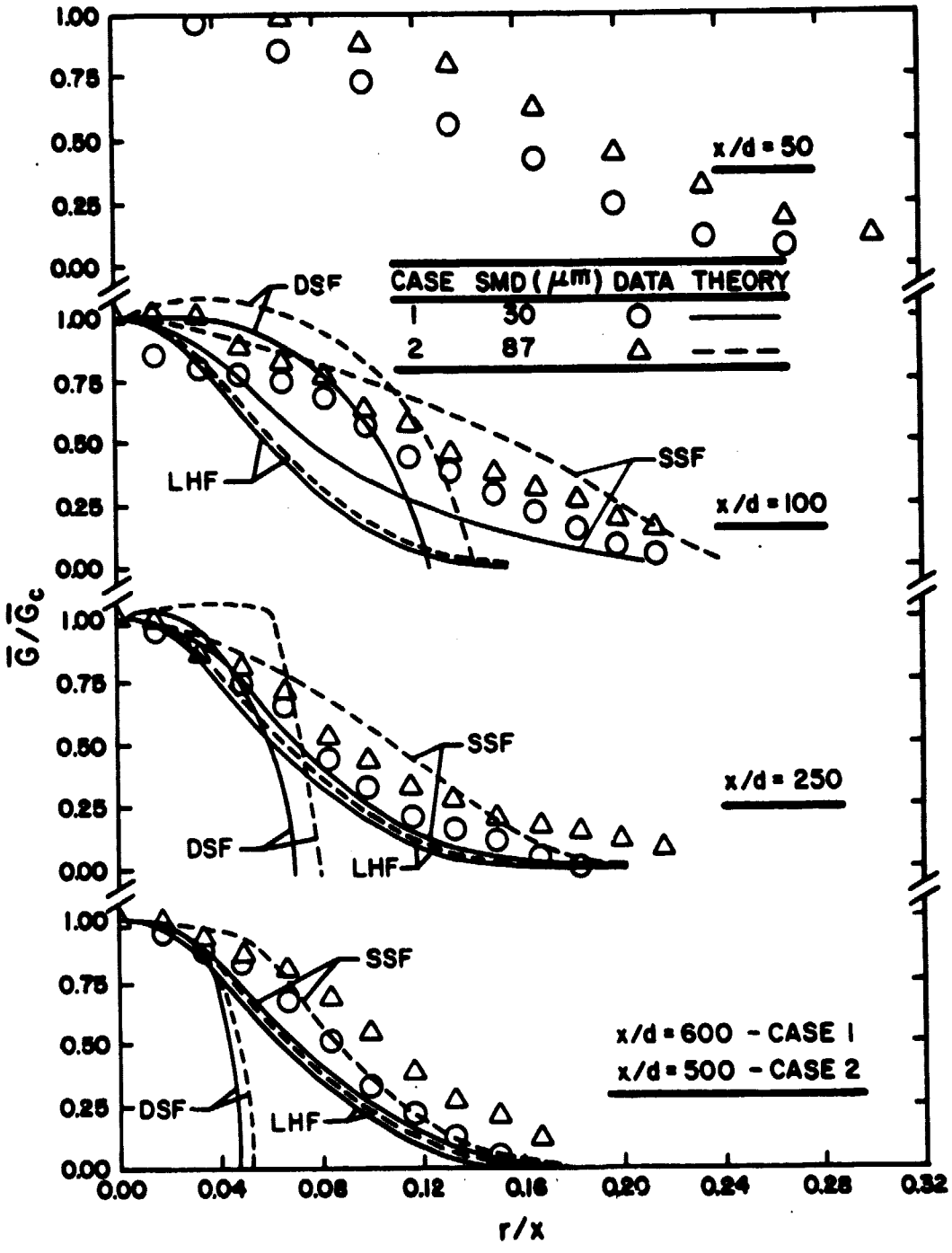

Fig. 20. Predicted and measured radial variation of mean-liquid flux in the nonevaporating sprays.

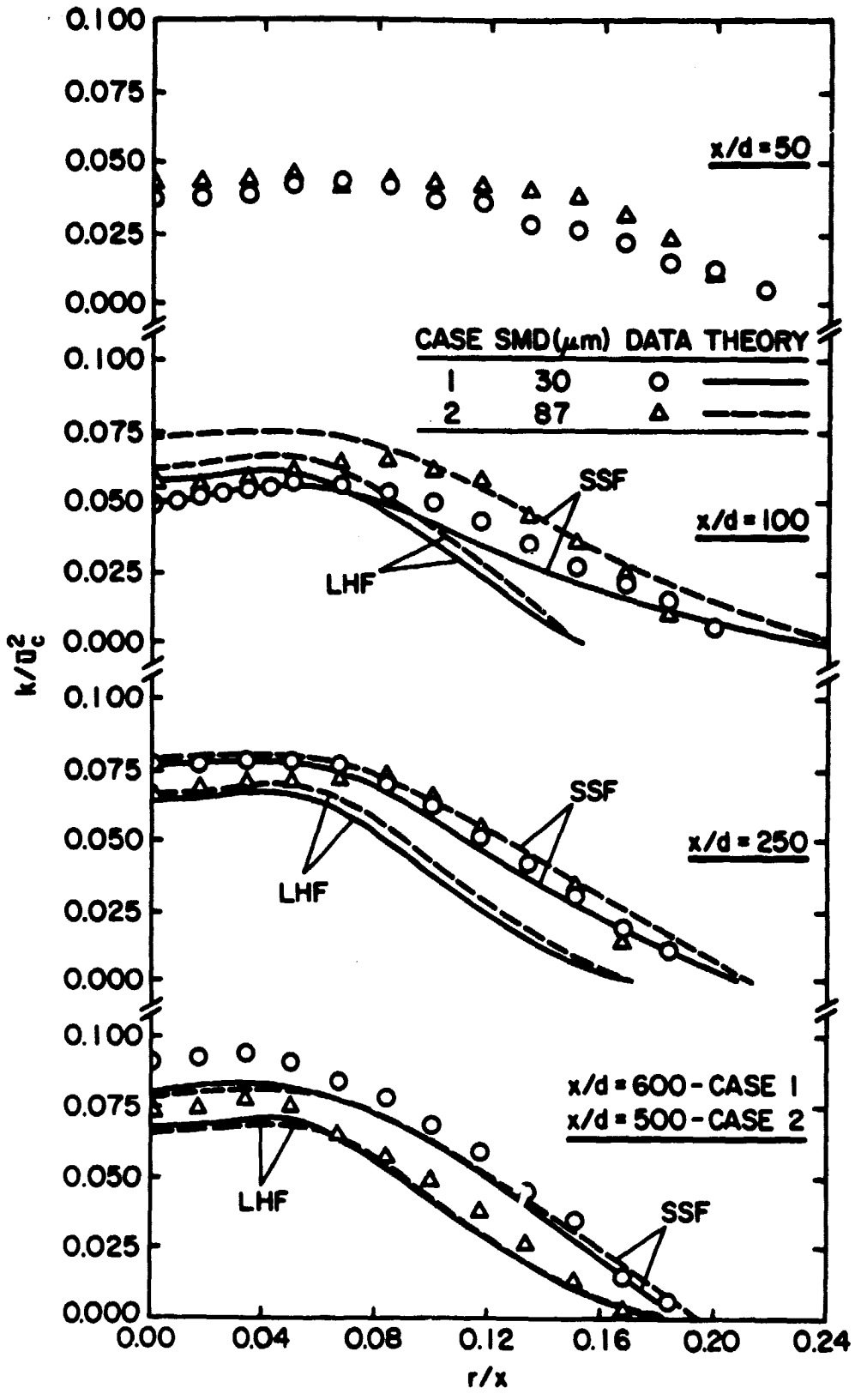

Fig. 21. Predicted and measured radial variation of k in the nonevaporating sprays.

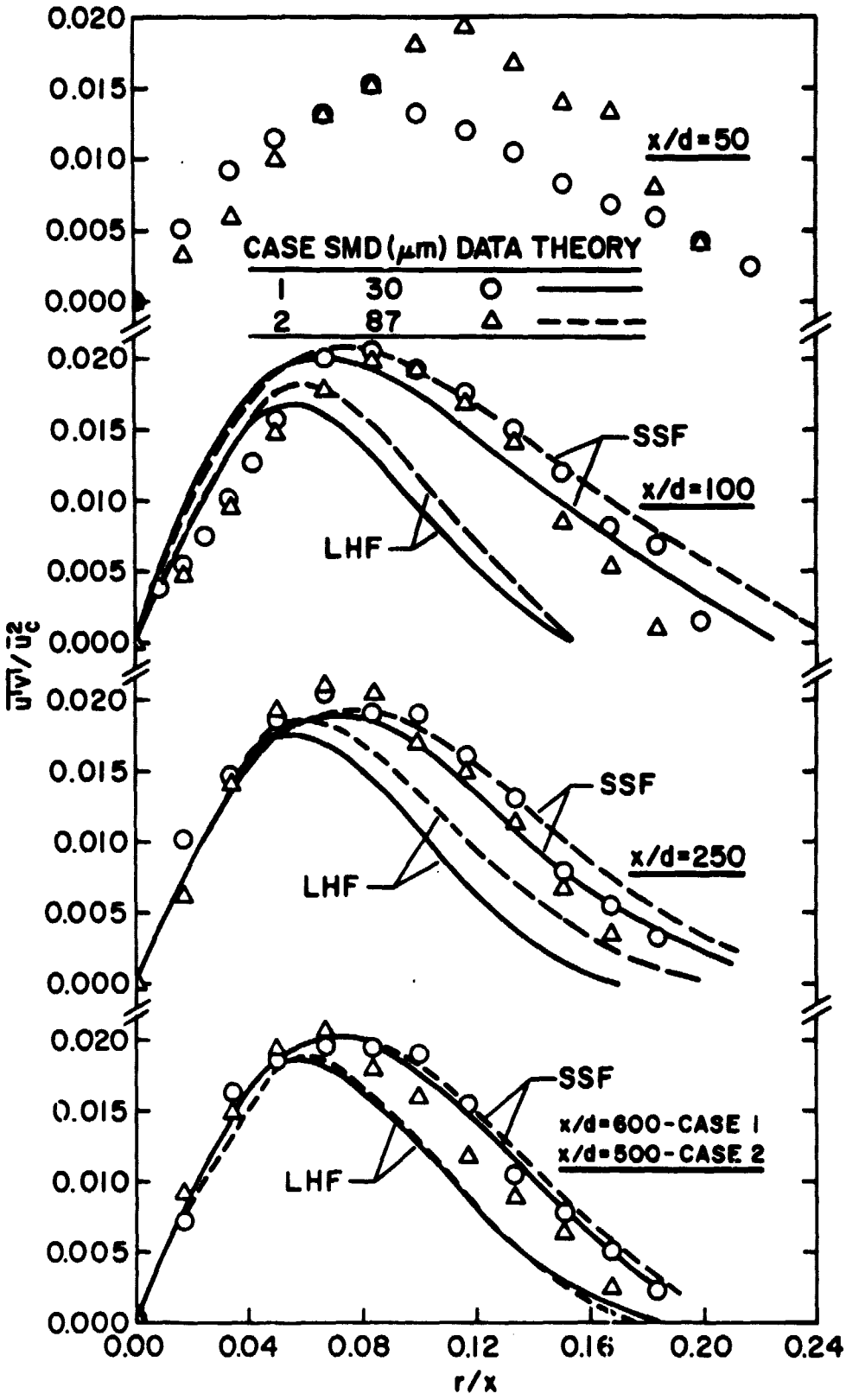

Fig. 22. Predicted and measured radial variation of Reynolds stress in the nonevaporating sprays.

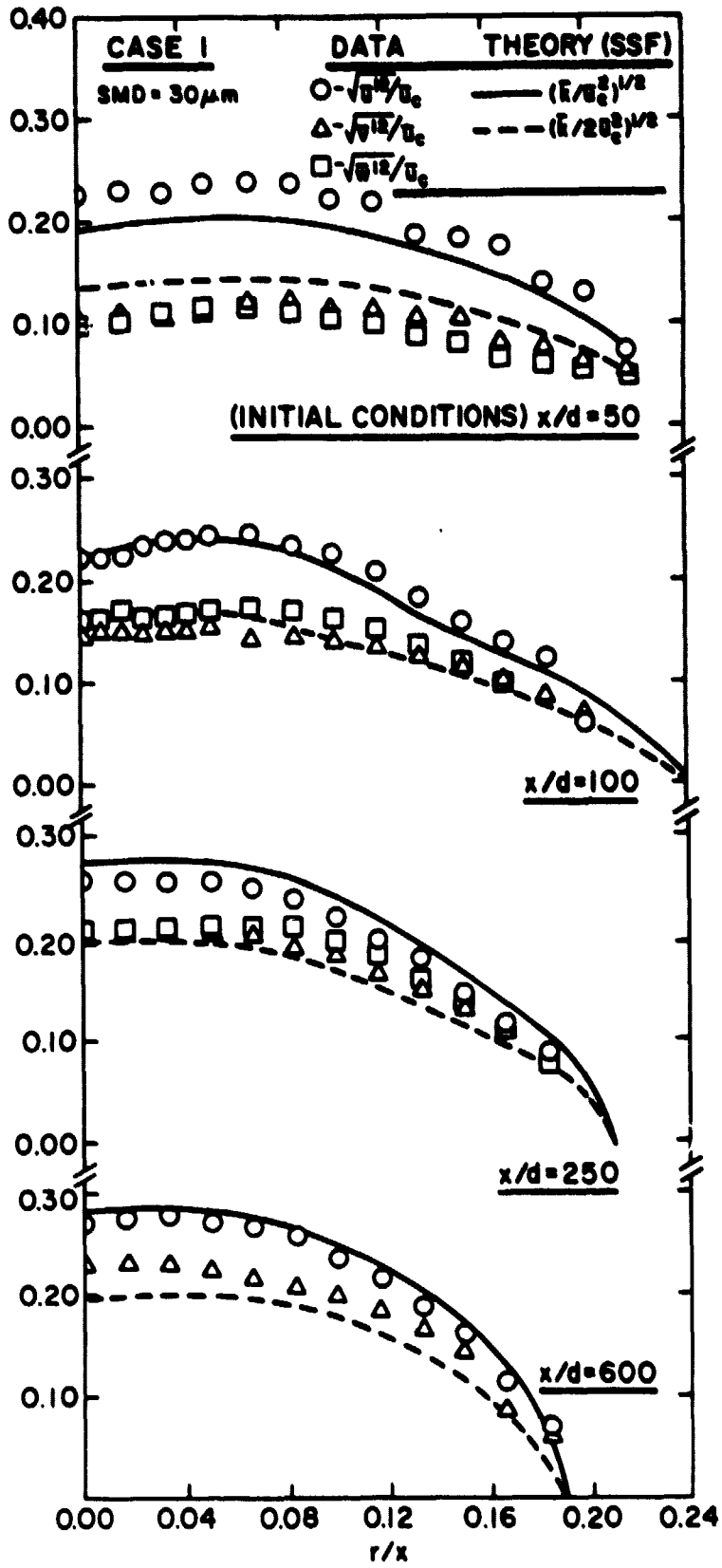

Fig. 23. Predicted and measured radial variation of velocity fluctuations for the case 1 spray (SMD = 30 μm).

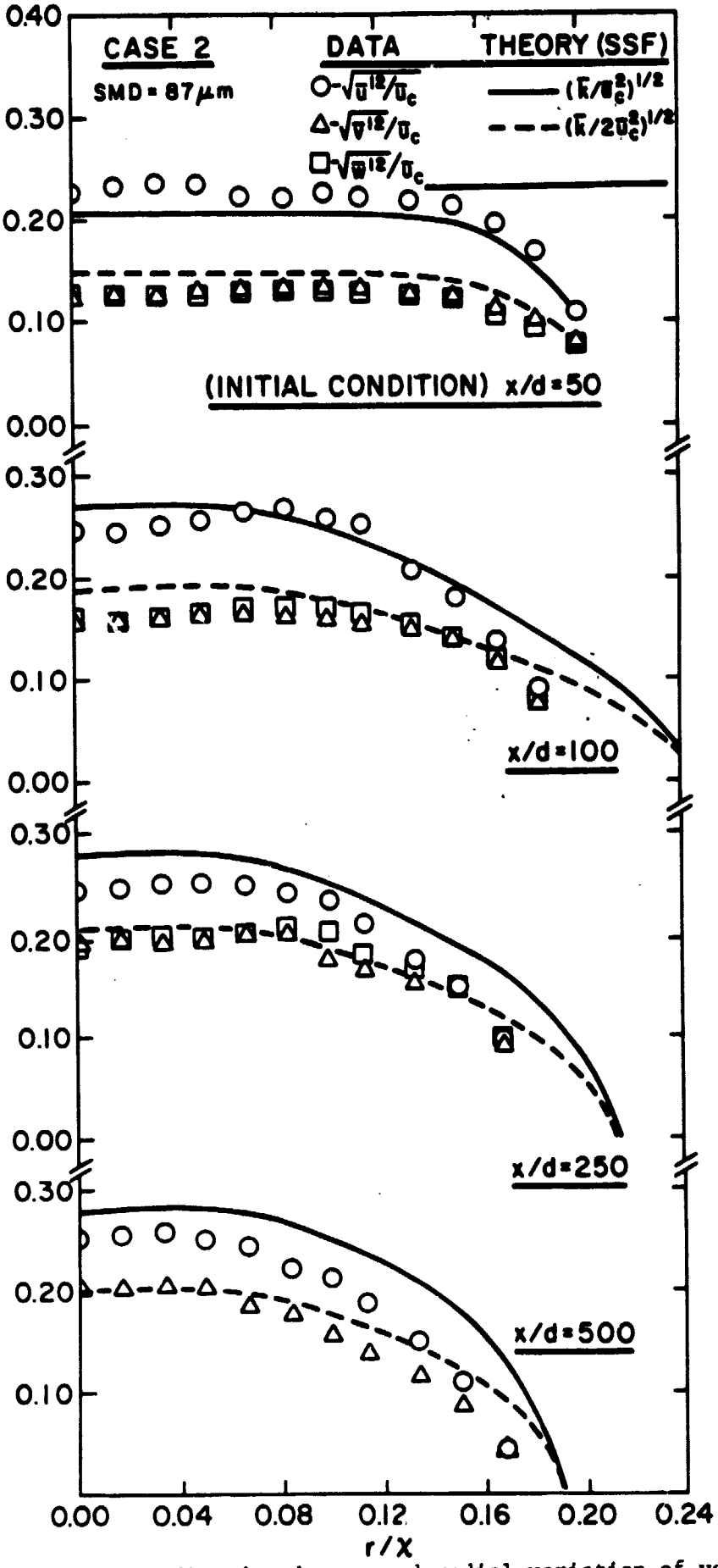

ORIGINAL PAGE IS
OF POOR QUALITY

Fig. 24. Predicted and measured radial variation of velocity fluctuations for the case 2 spray (SMD = 87 μm).

injector and generally exceed levels observed for comparable values of x/d in single-phase jets [26,32]. Since this region abuts the dense-spray portion of the flow, it seems likely that the presence of drops are responsible for the higher degree of anisotropy since effects of slip are preferentially transmitted into the streamwise velocity component. High levels of anisotropy are also of concern regarding the prescription of eddy properties in the present SSF model, since this approach is based on the assumption of isotropic turbulence. This suggests that multistress models of particle-laden flows might profitably be examined in order to gain more insight concerning effects of particles on turbulence properties.

6. SUMMARY AND CONCLUSIONS

New measurements of mean and fluctuating gas velocities, drop sizes and liquid fluxes were completed in the dilute portions of nonevaporating sprays in a still environment. These results were combined with existing measurements of the structure of particle-laden jets to evaluate models of the two-phase, jet-like flows. Three models were considered, as follows: (1) a locally homogeneous flow (LHF) model, where slip between the phases is neglected; (2) a deterministic separated flow (DSF) model, where interphase slip is considered but turbulent dispersion of particles is neglected; and (3) a stochastic separated flow (SSF) model, modified slightly from a proposal by Gosman and Ioannides [12], which allows for both interphase slip and the dispersion of particles by turbulent fluctuations. All three models employed a well-calibrated k-ε model for predictions of continuous-phase properties [1,5-7,16]. Two versions of the SSF model were considered, one computing the transit time of a particle through an eddy using a linearized procedure similar Gosman and Ioannides [12], the other allowing for nonlinear effects in transit time evaluations.

The LHF model was satisfactory for flows containing tracer-like particles, but was unsatisfactory for most practical flows. For particle-laden jets, the LHF model generally overestimated the rate of flow development and dispersion of particles, similar to past experience with this model [5-7]. For the nonevaporating sprays, however, the LHF model underestimated flow widths--unlike the results of earlier work. Such enhanced turbulent dispersion of particles, for certain ranges of turbulence and particle properties, is often observed in multiphase flows. The effect was more evident for the present sprays than for the particle-laden jets due to the smaller density of the liquid, which allowed the drops to respond more readily to turbulent fluctuations; and greater initial slip and rates of deceleration in the sprays, due to smaller injector dimensions. Due to the possibility of preferential dispersion under some conditions, we conclude that the LHF model does not always provide an upper bound on the rate of development of sprays, as suggested in the past [1].

The DSF model generally underestimated the rate of flow development and particle dispersion for the present data base. This approach appears to have limited utility for modeling practical particle-laden flows. Gosman and Ioannides [12] note, however, that uncertainties in initial conditions for multiphase flows are potentially a greater source of error than neglecting particle dispersion.

In contrast, the SSF models yielded reasonably good results over the present data base. In particular, the nonlinear version requires only a slightly more computational effort than the linearized version, while generally yielding improved predictions. The greatest discrepancies between predictions of the SSF models and the measurements in particle-laden jets were observed at high particle loadings. Uncertainties in initial conditions of the experiments are a major factor in these discrepancies, e.g., potential Magnus effects discussed by Laats and Frishman [24,24] for their measurements and particle velocity fluctuations at the jet exit for the measurements of Levy and Lockwood [25]. Effects of turbulence modulation, discussed by Al Taweel and Landau [31] or turbulence generation by particles may also contribute to errors at high particle mass loadings. The SSF models also provided adequate treatment of enhanced particle dispersion in the spray with no modification of the model from its original calibration (where effects of enhanced dispersion were not observed). While this is encouraging, additional evaluation of the model is needed--particularly considering improved specifications of initial conditions and measurements of drop sizes and velocities throughout the flow. Work along these lines is currently in progress in this laboratory.

Present measurements were limited to the dilute portion of the flows, where void fractions were greater than 99.1%. In this region, major effects of particles/drops on turbulence properties were not observed. As the dense particulate flow region was approached, however, turbulent velocity fluctuations exhibited increased anisotropy--suggesting a significant modification of turbulence properties by particles. The present SSF model, which employs assumptions of isotropy, still performed reasonably well in spite of this effect. However, further consideration of effects of anisotropy, perhaps using a multistress turbulence model, would be desirable. Further development of the model is also needed to consider direct effects of particles on the turbulence properties of the continuous phase.

Based on experience to date, the SSF method appears to provide an attractive formulation for treating nonlinear interphase transport phenomena in sprays. Extension of this approach to treat processes of drop heat-up and evaporation in sprays is currently being considered in this laboratory.

REFERENCES

1. Faeth, G. M., "Evaporation and Combustion of Sprays," Prog. in Energy and Combust. Sci., in press.

2. Alpert, R. L. and Mathews, M. K., "Calculation of Large-Scale Flow Fields Induced by Droplet Sprays," Polyphase Flow and Transport Technology, American Society of Mechanical Engineers, New York, 1980, pp. 112-128.

3. Alpert, R. L., "Calculated Interaction of Sprays with Large-Scale Buoyant Flows," ASME Paper No. 82-WA/HT-16, 1982.

4. Yule, A. J., Ah Seng, C., Felton, P. G., Ungut, A. and Chigier, N. A., "A Study of Vaporizing Sprays by Laser Techniques," Combustion and Flame, Vol. 44, 1982, pp. 71-84.

5. Shearer, A. J., Tamura, H. and Faeth, G. M., "Evaluation of a Locally Homogeneous Flow Model of Spray Evaporation," J. of Energy, Vol. 3, September-October 1979, pp. 271-278.

6. Mao, C-P., Szekely, G. A., Jr. and Faeth, G. M., "Evaluation of a Locally Homogeneous Flow Model of Spray Combustion," J. of Energy, Vol. 4, March-April 1980, pp. 78-87.

7. Mao, C-P., Wakamatsu, Y. and Faeth, G. M., "A Simplified Model of High Pressure Spray Combustion," Eighteenth Symposium (International) on Combustion, The Combustion Institute, Pittsburgh, 1981, pp. 337-347.

8. El Banhawy, Y. and Whitelaw, J. H., "Calculation of the Flow Properties of a Confined Kerosene-Spray Flame," AIAA J., Vol. 18, December 1980, pp. 1503-1510.

9. Mongia, H. C. and Smith, K., "An Empirical/Analytical Design Methodology for Gas Turbine Combustors," AIAA Paper No. 78-998, 1978.

10. Boyson, F. and Swithenbank, J., "Spray Evaporation in Recirculating Flow," Seventeenth Symposium (International) on Combustion, The Combustion Institute, Pittsburgh, 1979, pp. 443-453.

11. Yuu, S., Yasukouchi, N., Hirosawa, Y. and Jotaki, T., "Particle Turbulent Diffusion in a Dust Laden Round Jet," AIChE J., Vol. 24, 1978, pp. 509-519.

12. Gosman, A. D. and Ioannides, E., "Aspects of Computer Simulation of Liquid-Fueled Combustors," AIAA Paper No. 81-0323, 1981.

13. Shuen, J-S., Chen, L-D. and Faeth, G. M., "Evaluation of a Stochastic Model of Particle Dispersion in a Turbulent Round Jet," AIChE J., Vol. 29, 1983, pp. 167-170.

14. Shuen, J-S., Chen, L-D. and Faeth, G. M., "Predictions of the Structure of Turbulent, Particle-Laden, Round Jets," AIAA Paper No. 83-0066, 1983.

15. Solomon, A.S.P., Shuen, J-S., Zhang, Q-F. and Faeth, G. M., "Measurements and Predictions for Nonevaporating Sprays in a Quiescent Environment," AIAA Paper No. 83-0151, 1983

16. Lockwood, F. C. and Naguib, A. S., "The Prediction of the Fluctuations in the Properties of Free, Round-Jet, Turbulent, Diffusion Flames," Combustion and Flame, Vol. 24, 1975, pp. 109-124.

17. Schlicting, H., Boundary Layer Theory, McGraw-Hill Book Co., New York, 1979, p. 599.

18. Hinze, J. O., Turbulence, 2nd Ed., McGraw-Hill, New York, 1975, p. 427; also pp. 724-734.

19. Spalding, D. B., GENMIX: A General Computer Program for Two-Dimensional Parabolic Phenomena, Pergamon Press, Oxford, 1977.

20. Snyder, W. H. and Lumley, J. L., "Some Measurements of Particle Velocity Autocorrelation Functions in a Turbulent Flow," J. Fluid Mech., Vol. 48, 1971, pp. 41-71.

21. McComb, W. D. and Salih, S. M., "Measurement of Normalized Radial Concentration Profiles in a Turbulent Aerosol Jet Using a Laser-Doppler Anemometer," J. Aerosol Sci., Vol. 8, 1977, pp. 171-181.

22. McComb, W. D. and Salih, S. M., "Comparison of Some Theoretical Concentration Profiles for Solid Particle Measurements Using a Laser-Doppler Anemometer," J. Aerosol Sci., Vol. 9, 1978, pp. 299-313.

23. Laats, M. K. and Frishman, F. A., "Assumptions Used in Calculating the Two-Phase Jet," Fluid Dynamics, Vol. 5, 1970, pp. 333-338.

24. Laats, M. K. and Frishman, F. A., "Scattering of an Inert Admixture of Different Grain Size in a Two-Phase Axisymmetric Jet." Heat Transfer-Soviet Res., Vol. 2, 1970, pp. 7-12.

25. Levy, Y. and Lockwood, F. C., "Velocity Measurements in a Particle Laden Turbulent Free Jet," Combustion and Flame, Vol. 40, 1981, pp. 333-339.

26. Wygnanski, I. and Fiedler, H., "Some Measurements in a Self Preserving Jet," Journal of Fluid Mechanics, Vol. 38, 1969, pp. 577-612.

27. Becker, H. A., Hottell, H. C. and Williams, G. C., "The Nozzle-Fluid Concentration Field of Round, Turbulent, Free Jet," Journal of Fluid Mechanics, Vol. 30, 1967, pp. 285-303.

28. Corrsin, S. and Uberoi, M. S., "Further Experiments on the Flow and Heat Transfer in a Heated Turbulent Air Jet," NACA Report No. 998, 1950.

29. Hetsroni, G. and Sokolov, M., "Distribution of Mass Velocity, and Intensity of Turbulence in a Two-Phase Turbulent Jet," ASME Transactions, Journal of Applied Mechanics, Vol. 38, 1971, pp. 314-327.

30. Gosman, A. D., personal communication, 1982.

31. Al Tawell, A. M. and Landau, J., "Turbulence Modulation in Two-Phase Jets," Intl. J. Multiphase Flow, Vol. 3, 1977, pp. 341-351.

32. Rodi, W., "The Prediction of Free Turbulent Boundary Layers by use of a 2-Equation Turbulence Model," Ph.D. Thesis, University of London, 1972; also cited in Launder, B. E. and Morse, A., 'Numerical Prediction of Axisymmetric Free Shear Flows with a Reynolds Stress Closure," Turbulent Shear Flows I, (F. Durst, et al., ed.), Springer-Verlag, Berlin, 1979, pp. 279-294.

APPENDIX A

Data for the Nonevaporating Spray (Case 1)

A.1 Gas Phase

Table A.1 Axial Variation of Centerline Velocity

x/d	$\bar{u}_c/\bar{u}_o$
40	0.236
50	0.204
70	0.159
100	0.118
150	0.083
250	0.050
400	0.031
600	0.022

Table A.2 Radial Variation of Quantities

x/d = 50

r/x	$\bar{u}/\bar{u}_c$	$\overline{u'v'}/\bar{u}_c^2$	$\sqrt{\bar{u}'^2}/\bar{u}_c$	$\sqrt{\bar{v}'^2}/\bar{u}_c$	$\sqrt{\bar{w}'^2}/\bar{u}_c$	$\bar{k}/\bar{u}_c^2$
0.0	1.0	0.0	0.229	0.104	0.099	.0365
0.017	0.983	.0051	0.231	0.108	0.101	.0375
0.034	0.952	.0091	0.229	0.110	0.112	.0386
0.050	0.886	.0116	0.238	0.113	0.118	.0416
0.067	0.799	.0134	0.239	0.124	0.117	.0431
0.084	0.722	.0153	0.238	0.123	0.112	.0421
0.101	0.654	.0132	0.222	0.116	0.106	.0371
0.117	0.557	.0120	0.221	0.116	0.099	.0359
0.134	0.422	.0104	0.189	0.109	089	.0279
0.151	0.357	.0082	0.186	0.108	[illegible]	.0264
0.168	0.277	.0069	0.178	0.086	0.069	.0220
0.184	0.233	.0060	0.141	0.080	0.064	.0151
0.201	0.180	.0046	0.133	0.066	0.057	.0127
0.218	0.085	.0025	0.075	0.060	0.051	.0059

Table A.3 Radial Variation of Quantities

x/d = 100

r/x	$\bar{u}/\bar{u}_c$	$\overline{u'v'}/\bar{u}_c^2$	$\sqrt{\bar{u}'^2}/\bar{u}_c$	$\sqrt{\bar{v}'^2}/\bar{u}_c$	$\sqrt{\bar{w}'^2}/\bar{u}_c$	$\bar{k}/\bar{u}_c^2$
0.0	1.0	0.0	0.224	0.147	0.161	.048º
0.008	0.988	.0039	0.224	0.151	0.163	.0496
0.017	0.982	.0053	0.226	0.151	0.173	.0521
0.025	0.961	.0076	0.236	0.150	0.165	.0528
0.034	0.932	.0100	0.240	0.151	0.166	.0541
0.042	0.885	.0127	0.240	0.153	0.169	.0552
0.050	0.832	.0157	0.246	0.156	0.171	.0571
0.067	0.717	.0199	0.247	0.144	0.174	.0559
0.084	0.602	.0202	0.236	0.146	0.172	.0533
0.101	0.515	.0195	0.228	0.141	0.165	.0497
0.117	0.409	.0175	0.209	0.137	0.156	.0433
0.134	0.310	.0149	0.186	0.128	0.138	.0351
0.151	0.243	.0119	0.161	0.116	0.121	.0270
0.168	0.168	.0082	0.142	0.103	0.101	.0205
0.184	0.121	.0068	0.126	0.090	0.086	.0157
0.201	0.059	.0014	0.061	0.072	0.053	.0059

Table A.4 Radial Variation of Quantities

x/d = 250

r/x	$\bar{u}/\bar{u}_c$	$\overline{u'v'}/\bar{u}^2$	$\sqrt{\bar{u}'^2}/\bar{u}_c$	$\sqrt{\bar{v}'^2}/\bar{u}_c$	$\sqrt{\bar{w}'^2}/\bar{u}_c$	$\bar{k}/\bar{u}_c^2$
0.0	1.00	0.0	0.258	0.207	0.209	.0764
0.017	0.981	.0101	0.257	0.209	0.211	.0771
0.034	0.923	.0146	0.257	0.210	0.214	.0781
0.050	0.799	.0185	0.257	0.206	0.216	.0776
0.067	0.709	.0202	0.251	0.207	0.216	.0762
0.084	0.597	.0190	0.239	0.194	0.212	.0698
0.101	0.487	.0189	0.223	0.185	0.198	.0616
0.117	0.389	.0159	0.200	0.169	0.184	.0513
0.134	0.297	.0129	0.181	0.152	0.163	.0411
0.151	0.191	.0079	0.147	0.133	0.142	.0297
0.168	0.146	.0055	0.118	0.109	0.106	.0185
0.184	0.104	.0032	0.091	0.091	0.078	.0112

Table A.5 Radial Variation of Quantities

$x/d = 600$

r/x	$\bar{u}/\bar{u}_c$	$\overline{u'v'}/\bar{u}_c^2$	$\sqrt{\bar{u}'^2}/\bar{u}_c$	$\sqrt{\bar{v}'^2}/\bar{u}_c$	$\bar{k}/\bar{u}_c^{2*}$
0.0	1.00	0.0	0.272	0.231	.0906
0.017	0.997	.0072	0.277	0.233	.0928
0.034	0.957	.0162	0.281	0.233	.0936
0.050	0.869	.0185	0.274	0.230	.0905
0.067	0.778	.0195	0.269	0.218	.0841
0.084	0.666	.0196	0.259	0.210	.0777
0.101	0.546	.0189	0.237	0.201	.0684
0.117	0.446	.0153	0.219	0.186	.0589
0.134	0.313	.0104	0.187	0.167	.0454
0.151	0.228	.0079	0.163	0.147	.0349
0.168	0.166	.0050	0.116	0.089	.0148
0.184	0.087	.0022	0.070	0.061	.00612

*Calculated assuming $\sqrt{\bar{w}'^2} = \sqrt{\bar{v}'^2}$

A.2 Liquid Phase

Table A.6 Axial Variation of Centerline Liquid Flux

x/d	$\bar{G}_c/\bar{G}_o \times 10^3$
40	5.25
50	3.72
70	2.65
100	1.45
150	0.96
250	0.41
400	0.19
600	0.08

Table A.7 Radial Variation of Liquid Flux

r/x	x/d = 50 $\bar{G}/\bar{G}_c$	100 $\bar{G}/\bar{G}_c$	250 $\bar{G}/\bar{G}_c$	600 $\bar{G}/\bar{G}_c$
0.0	1.00	1.00	1.00	1.00
0.017	--	0.85	0.97	0.97
0.034	0.97	0.80	0.90	0.90
0.050	--	0.77	0.75	0.83
0.067	0.85	0.75	0.65	0.67
0.084	--	0.68	0.44	0.50
0.101	0.73	0.56	0.33	0.32
0.117	--	0.44	0.20	0.21
0.134	0.56	0.38	0.16	0.12
0.151	--	0.29	0.12	0.05
0.168	0.42	0.21	0.05	--
0.184	--	0.15	0.01	--
0.201	0.24	0.08	--	--
0.218	--	0.05	--	--
0.235	0.11	--	--	--
0.268	0.07	--	--	--

Table A.8 Radial Variation of Drop Size Distributions at x/d = 50
(Entries are Relative Percentage Number Frequency)

Diameter	0.00	6.36	12.72	19.08	25.44	31.80	38.16	44.52	50.88	57.24
Size Range	--	--	--	--	--	--	--	--	--	--
(μm)	6.36	12.72	19.08	25.44	31.80	38.16	44.52	50.88	57.24	63.6
r/x										
0.00	19.95	19.90	18.6	18.6	7.8	7.8	2.15	2.15	0.9	0.9
0.050	13.4	20.0	31.1	15.1	8.1	4.5	2.1	1.9	1.1	0.65
0.084	8.5	23.3	37.5	13.8	6.3	3.9	2.1	1.3	0.88	0.60
0.117	18.0	34.2	24.5	8.3	5.3	2.6	1.5	1.4	0.92	0.76
0.151	20.6	31.2	16.5	8.7	3.5	2.3	1.6	1.3	0.78	0.54
0.184	27.0	25.1	24.6	9.7	3.8	2.7	1.8	1.1	1.2	0.70
0.218	20.5	51.3	15.6	5.4	2.5	1.7	0.53	0.53	0.23	0.23
0.251	29.6	44.3	14.2	5.7	1.9	0.68	0.68	0.68	0.95	0.27

(Continued)

Table A.8 Radial Variation of Drop Size Distributions at x/d = 50

(Entries are Relative Percentage Number Frequency)

Diameter	63.60	69.96	76.32	82.68	89.04	95.40	101.8	108.1	114.5
Size Range	--	--	--	--	--	--	--	--	--
(μm)	69.96	76.32	82.68	89.04	95.40	101.8	108.1	114.5	120.8
r/x									
0.00	0.37	0.37	0.11	0.11	0.08	0.08	0.02	0.02	0.00
0.050	0.32	0.29	0.19	0.23	0.10	0.03	0.06	0.06	0.06
0.084	0.35	0.25	0.11	0.18	0.21	0.14	0.14	0.14	0.14
0.117	0.32	0.36	0.28	0.08	0.32	0.28	0.20	0.00	0.12
0.151	0.49	0.44	0.49	0.19	0.39	0.19	0.00	0.00	0.00
0.184	0.39	0.47	0.31	0.39	0.00	0.23	0.16	0.00	0.08
0.218	0.15	0.15	0.23	0.08	0.15	0.23	0.08	0.00	0.08
0.251	0.27	0.00	0.00	0.27	0.14	0.00	0.00	0.27	0.00

Table A.9 Radial Variation of SMD at x/d = 50

r/x	SMD (μm)
0.00	40.6
0.050	41.8
0.084	46.2
0.117	50.7
0.151	49.3
0.184	9.4
0.218	43.6
0.251	47.6

APPENDIX B

Data for the Nonevaporating Spray (Case 2)

B.1 Gas Phase

Table B.1 Axial Variation of Centerline Velocity

x/d	$\bar{u}_c/\bar{u}_o$
40	0.490
50	0.447
70	0.338
100	0.249
150	0.182
250	0.118
400	0.078
500	0.066
600	0.060

Table B.2 Radial Variation of Quantities

x/d = 50

r/x	$\bar{u}/\bar{u}_c$	$\overline{u'v'}/\bar{u}_c^2$	$\sqrt{\bar{u}'^2}/\bar{u}_c$	$\sqrt{\bar{v}'^2}/\bar{u}_c$	$\sqrt{\bar{w}'^2}/\bar{u}_c$	$\bar{k}/\bar{u}_c^2$
0.0	1.000	0.00	0.228	0.125	0.126	.0416
0.017	0.998	.0034	0.234	0.127	0.126	.0434
0.034	0.956	.0060	0.236	0.128	0.127	.0441
0.050	0.924	.0103	0.235	0.132	0.130	.0448
0.067	0.829	.0132	0.222	0.134	0.132	.0422
0.084	0.773	.0152	0.222	0.136	0.133	.0429
0.101	0.693	.0179	0.226	0.136	0.133	.0434
0.117	0.614	.0196	0.222	0.134	0.130	.0420
0.134	0.550	.0166	0.220	0.129	0.128	.0408
0.151	0.462	.0140	0.216	0.127	0.122	.0388
0.168	0.391	.0133	0.198	0.114	0.105	.0316
0.184	0.267	.0080	0.169	0.104	0.094	.0241
0.201	0.148	.0041	0.110	0.081	0.078	.0124

ORIGINAL PAGE IS OF POOR QUALITY

Table B.3 Radial Variation of Quantities

x/d = 100

r/x	$\bar{u}/\bar{u}_c$	$\overline{u'v'}/\bar{u}_c^2$	$\sqrt{\bar{u}'^2}/\bar{u}_c$	$\sqrt{\bar{v}'^2}/\bar{u}_c$	$\sqrt{\bar{w}'^2}/\bar{u}_c$	$\bar{k}/\bar{u}_c^2$
0.0	1.00	0.00	0.248	0.157	0.163	.0564
0.017	0.998	.0046	0.247	0.159	0.159	.0558
0.034	0.972	.0096	0.252	0.161	0.162	.0576
0.050	0.899	.0149	0.258	0.164	0.166	.0605
0.067	0.836	.0179	0.266	0.166	0.171	.0637
0.084	0.745	.0199	0.269	0.164	0.172	.0645
0.101	0.656	.0192	0.259	0.162	0.172	.0613
0.117	0.548	.0169	0.252	0.156	0.166	.0576
0.134	0.447	.0142	0.208	0.149	0.155	.0447
0.151	0.333	.0086	0.181	0.138	0.141	.0359
0.168	0.159	.0054	0.138	0.117	0.121	.0237
0.184	0.113	.0010	0.089	0.076	0.088	.0108

Table B.4 Radial Variation of Quantities

x/d = 250

r/x	$\bar{u}/\bar{u}_c$	$\overline{u'v'}/\bar{u}_c^2$	$\sqrt{\bar{u}'^2}/\bar{u}_c$	$\sqrt{\bar{v}'^2}/\bar{u}_c$	$\sqrt{\bar{w}'^2}/\bar{u}_c$	$\bar{k}/\bar{u}_c^2$
0.0	1.00	0.0	0.246	0.192	0.189	.0663
0.017	0.983	.0061	0.248	0.196	0.197	.0694
0.034	0.923	.0141	0.251	0.193	0.199	.0700
0.050	0.863	.0192	0.253	0.195	0.198	.0706
0.067	0.739	.0209	0.251	0.201	0.203	.0722
0.084	0.644	.0203	0.241	0.203	0.209	.0716
0.101	0.517	.0169	0.234	0.177	0.203	.0636
0.117	0.453	.0149	0.211	0.169	0.181	.0530
0.134	0.336	.0113	0.176	0.154	0.167	.0414
0.151	0.199	.0067	0.149	0.146	0.150	.0331
0.168	0.121	.0035	0.099	0.090	0.101	.0141

Table B.5 Radial Variation of Quantities

x/d = 500

r/x	$\bar{u}/\bar{u}_c$	$\overline{u'v'}/\bar{u}_c^2$	$\sqrt{\bar{u}'^2}/\bar{u}_c$	$\sqrt{\bar{w}'^2}/\bar{u}_c$	$\bar{k}/\bar{u}_c^{2*}$
0.00	1.000	0.0	0.255	0.204	.0742
0.017	0.985	.0091	0.258	0.202	.0741
0.034	0.939	.0148	0.261	0.207	.0768
0.050	0.866	.0194	0.254	0.205	.0745
0.067	0.813	.0206	0.246	0.187	.0652
0.084	0.646	.0180	0.224	0.180	.0575
0.101	0.532	.0160	0.214	0.159	.0483
0.117	0.365	.0118	0.190	0.140	.0378
0.134	0.251	.0089	0.150	0.119	.0257
0.151	0.163	.0063	0.110	0.088	.0138
0.168	0.069	.0024	0.045	0.046	.0032

*Calculated assuming $\sqrt{\bar{w}'^2} = \sqrt{\bar{v}'^2}$

B.2 Liquid Phase

Table B.6 Axial Variation of Centerline Liquid Flux

x/d	$\bar{G}_c/\bar{G}_o \times 10^3$
40	3.24
50	2.13
70	1.34
100	0.99
150	0.50
250	0.25
400	0.12
500	0.076

Table B.7 Radial Variation of Liquid Flux

r/x	$\frac{x/d = 50}{\bar{G}/\bar{G}_c}$	$\frac{100}{\bar{G}/\bar{G}_c}$	$\frac{250}{\bar{G}/\bar{G}_c}$	$\frac{500}{\bar{G}/\bar{G}_c}$
0.0	1.00	1.00	1.00	1.00
0.017	--	1.01	0.99	0.98
0.034	0.97	0.99	0.87	0.92
0.050	--	0.88	0.80	0.85
0.067	0.99	0.81	0.70	0.80
0.084	--	0.76	0.52	0.68
0.101	0.88	0.63	0.43	0.55
0.117	--	0.57	0.32	0.39
0.134	0.80	0.45	0.27	0.27
0.151	--	0.37	0.20	0.20
0.168	0.62	0.31	0.16	0.12
0.184	--	0.26	0.14	--
0.201	0.44	0.20	0.10	--
0.218	--	0.16	0.07	--
0.235	0.20	--	--	--
0.268	0.13	--	--	--

Table B.8 Radial Variation of Drop Size Distributions at x/d = 50
(Entries are Relative Percentage Number Frequency)

Diameter	0.00	6.36	12.72	19.08	25.44	31.80	38.16	44.52	50.88	57.24	63.60
Size Range	--	--	--	--	--	--	--	--	--	--	--
(μm)	6.36	12.72	19.08	25.44	31.80	38.16	44.52	50.88	57.24	63.60	69.96
r/x											
0.00	0.0	10.1	33.9	16.8	8.1	5.7	5.3	3.0	1.0	0.67	1.0
0.050	0.0	3.1	19.5	23.3	12.2	7.3	5.7	5.3	3.4	1.5	2.3
0.084	0.0	4.9	22.1	17.2	12.9	9.2	6.7	4.3	1.2	3.1	2.5
0.117	0.0	8.7	21.7	11.2	14.3	8.1	8.1	6.8	1.9	0.6	2.5
0.151	0.0	9.4	16.4	10.9	14.1	10.9	4.7	8.6	2.3	5.5	2.3
0.184	0.0	17.1	20.0	7.1	11.4	4.3	0.0	4.3	4.3	8.6	2.9
0.218	0.0	41.8	28.4	6.0	4.5	0.0	2.9	0.0	2.9	2.9	0.0

(Continued)

Table B.8 Radial Variation of Drop Size Distributions at x/d = 50

(Entries are Relative Percentage Number Frequency)

Diameter	69.96	76.32	82.68	89.04	95.40	101.8	108.1	114.5	120.8	127.2	133.6
Size Range	--	--	--	--	--	--	--	--	--	--	--
(μm)	76.32	82.68	89.04	95.40	101.8	108.1	114.5	120.8	127.2	133.6	139.9
r/x											
0.00	1.6	2.6	1.0	1.3	0.7	0.7	0.7	0.3	1.3	0.3	1.0
0.050	3.8	0.8	1.9	1.1	1.1	0.8	0.8	0.4	1.5	1.1	0.0
0.084	0.0	1.3	1.3	0.6	1.3	1.3	0.6	0.0	1.3	0.6	0.6
0.117	1.2	0.62	2.5	0.0	1.9	1.2	0.6	0.6	0.0	0.6	0.0
0.151	0.0	0.78	3.1	1.6	1.6	1.6	1.6	0.0	0.8	0.0	0.0
0.184	5.7	0.0	5.7	1.4	0.0	0.0	1.4	0.0	0.0	1.4	0.0
0.218	4.5	0.0	4.5	0.0	0.0	0.0	0.0	0.0	0.0	0.0	0.0

(Continued)

Table B.8 Radial Variation of Drop Size Distributions at x/d = 50

(Entries are Relative Percentage Number Frequency)

Diameter	139.9	146.3	152.6	159.0	165.4	171.7	178.1	184.4	198.8	197.2
Size Range	--	--	--	--	--	--	--	--	--	--
(μm)	146.3	152.6	159.0	165.4	171.7	178.1	184.4	190.8	197.2	203.5
r/x										
0.00	0.7	0.0	1.0	0.3	0.0	0.3	0.0	0.3	0.0	0.3
0.050	0.4	0.4	0.0	0.4	0.0	0.4	0.4	0.4	0.0	0.8
0.084	0.6	0.6	0.0	0.6	0.0	0.0	0.0	1.2	1.2	0.0
0.117	0.6	1.2	0.6	0.6	0.0	0.6	1.9	0.0	1.2	0.0
0.151	0.8	0.8	0.8	0.8	0.0	0.8	0.0	0.0	0.0	0.8
0.184	0.0	1.4	1.4	0.0	0.0	0.0	0.0	0.0	0.0	1.4
0.218	0.0	0.0	0.0	1.5	0.0	0.0	0.0	0.0	0.0	0.0

Table B.9 Radial Variation of SMD at x/d = 50

r/x	SMD (μm)
0.00	111.1
0.050	109.3
0.084	116.6
0.117	126.9
0.151	100.8
0.184	112.1
0.218	91.1